EUROPEAN ORGANIZATION FOR NUCLEAR RESEARCH

CERN-EP-2020-218
10 November 2020

Λ_c^+ production in pp and in p–Pb collisions at $\sqrt{s_{NN}}$ = 5.02 TeV

ALICE Collaboration*

Abstract

The production cross section of prompt Λ_c^+ charmed baryons was measured with the ALICE detector at the LHC at midrapidity in proton-proton (pp) and proton-lead (p–Pb) collisions at a centre-of-mass energy per nucleon pair of $\sqrt{s_{NN}} = 5.02$ TeV. The Λ_c^+ and $\overline{\Lambda}_c^-$ baryons were reconstructed in the hadronic decay channels $\Lambda_c^+ \to pK^-\pi^+$ and $\Lambda_c^+ \to pK_S^0$ and respective charge conjugates. The measured differential cross sections as a function of transverse momentum (p_T) and the p_T-integrated Λ_c^+ production cross section in pp and in p–Pb collisions are presented. The Λ_c^+ nuclear modification factor (R_{pPb}), calculated from the cross sections in pp and in p–Pb collisions, is presented and compared with the R_{pPb} of D mesons. The Λ_c^+/D^0 ratio is also presented and compared with the light-flavour baryon-to-meson ratios p/π and Λ/K_S^0, and measurements from other LHC experiments. The results are compared to predictions from model calculations and Monte Carlo event generators.

*See Appendix A for the list of collaboration members

1 Introduction

In hadronic collisions, heavy quarks (charm and beauty) are created predominantly in hard scattering processes, and therefore the measurement of charm and beauty hadron production is a powerful test of perturbative quantum chromodynamics (pQCD) calculations. Theoretical predictions based on the QCD factorisation approach describe the heavy-flavour hadron production cross section as a convolution of parton distribution functions, parton hard-scattering cross sections, and fragmentation functions. The measurements of D- and B-meson production cross sections in pp collisions at centre-of-mass energies between 200 GeV and 13 TeV at RHIC, Tevatron, and the LHC are generally described within uncertainties by perturbative calculations at next-to-leading order with next-to-leading-log resummation, such as the general-mass variable-flavour-number scheme (GM-VFNS [1, 2]) and fixed-order next-to-leading-log (FONLL [3, 4]), over a wide range of transverse momentum (p_T).

The measurement of the relative production of different heavy-flavour hadron species is also sensitive to the charm- and beauty-quark hadronisation and heavy-flavour hadron formation processes. A measurement of Λ_c^+ baryon production at midrapidity in pp collisions at $\sqrt{s} = 7$ TeV was reported by the ALICE Collaboration in [5]. The Λ_c^+/D^0 ratio was found to be substantially higher than previous measurements at lower energies in electron-positron (e^+e^-) [6–9] and electron-proton (e^-p) [10–12] collisions, suggesting that the probabilities for a charm quark to hadronise into a specific charmed hadron (fragmentation fractions) are not universal among different collision systems. In addition, the Λ_c^+/D^0 ratio was compared with predictions from several Monte Carlo (MC) generators, which implement different fragmentation processes, such as the formation of strings (PYTHIA[13, 14]), ropes (DIPSY[15, 16]), or baryonic clusters (HERWIG[17]), where the fragmentation parameters for these simulations are tuned to previous e^+e^- and e^-p collision measurements. These predictions significantly underestimate the Λ_c^+/D^0 ratio, although the prediction from PYTHIA 8 that includes additional colour reconnection mechanisms [14] shows a p_T trend that is qualitatively similar to the measured trend. The CMS Collaboration has measured the Λ_c^+/D^0 ratio in pp collisions at $\sqrt{s} = 5.02$ TeV [18], which is consistent with predictions from PYTHIA 8 with additional colour reconnection mechanisms. Λ_c^+ production was also measured by the LHCb Collaboration in pp collisions at $\sqrt{s} = 7$ TeV at forward rapidity [19], and the Λ_c^+/D^0 ratio was found to be lower than that measured by ALICE at midrapidity [5]. Calculations of the charmed-hadron production cross section based on the k_T-factorisation approach with gluon distributions obtained on the basis of novel collinear gluon distribution functions and Peterson fragmentation functions [20] are unable to simultaneously describe the ALICE and LHCb measurements using the same set of input parameters, suggesting that the measurements are difficult to explain within the independent parton fragmentation scheme. It is also important to note here that the magnitude of the relative production of Λ_b^0 baryons and beauty mesons in pp collisions measured by LHCb [21–23] and CMS [24] offer further hints that fragmentation fractions in the beauty sector differ between collision systems.

The study of charm production in heavy-ion collisions is a powerful tool to investigate the quark–gluon plasma (QGP)[25–27], the deconfined state of matter created under extreme energy densities. In particular, the charmed baryon-to-meson ratio in heavy-ion collisions is sensitive to the charm hadronisation mechanisms after the QGP phase. It is expected that a significant fraction of low- and intermediate-momentum charm quarks hadronise via recombination (coalescence) with light (anti) quarks from the medium[28, 29], which would manifest as an enhancement of the Λ_c^+/D^0 ratio with respect to pp collisions. The Λ_c^+/D^0 ratio has been measured by STAR [30] in Au–Au collisions at $\sqrt{s_{NN}} = 200$ GeV, and by ALICE [31] and CMS [18] in Pb–Pb collisions at $\sqrt{s_{NN}} = 5.02$ TeV. These measurements offer constraints to different model calculations which implement contributions to hadronisation via quark recombination [32–35]. Measurements of the same observable in pp collisions provide a necessary reference for studies in heavy-ion collisions.

The interpretation of the results obtained in heavy-ion collisions also requires detailed studies in p–Pb collisions in order to assess so-called cold nuclear matter (CNM) effects in the initial and final states, which could modify the production of heavy-flavour hadrons. In the initial state, the quark and gluon distributions are modified in bound nucleons compared to free nucleons, depending on the fractional longitudinal parton momentum x and the atomic mass number [36, 37]. The most relevant CNM effect at LHC energies is shadowing, i.e. a decrease of the parton densities in the small-x region. This effect is due to high phase-space densities of low-x partons and can be described in collinear pQCD by means of parametrisations of the modification of the nuclear parton distribution functions (nPDFs) [38, 39]. In the case of saturation of the parton phase-space, the Colour Glass Condensate (CGC) effective theory [40–44] offers an appropriate theoretical framework to describe the modification of the nPDFs. Moreover, partons can lose energy in the initial stages of the collisions due to initial-state radiation [45], or experience transverse momentum broadening due to multiple soft collisions before the heavy-quark pair is created in the hard scattering [46–48]. The modification of parton distributions in the nucleus and energy loss in the initial state can affect the yields and the momentum distributions of the produced hadrons, mainly at low momenta. In addition to initial-state effects, final-state effects can also modify the hadron yields and momentum distributions. Several measurements in high-multiplicity pp and p–Pb collisions, such as long-range correlations of charged hadrons [49–52], and the enhancement of baryon-to-meson ratios in the light-flavour sector (p/π and Λ/K) [53–55], exhibit a similar behaviour as that observed in Pb–Pb collisions, suggesting that these findings may have similar physical origins in pp, p–A, and A–A collisions [56]. Λ_c^+ production was previously measured by ALICE in p–Pb collisions at $\sqrt{s_{NN}} = 5.02$ TeV [5]. The Λ_c^+/D^0 ratio was found to be compatible within the uncertainties with that measured in pp collisions at $\sqrt{s} = 7$ TeV. The nuclear modification factor, R_{pPb}, was found to be compatible with unity, as well as with models that implement cold nuclear matter effects via nPDF calculations [57] or assume the production of a deconfined medium in p–Pb collisions [58]. The LHCb Collaboration has measured the Λ_c^+/D^0 ratio at forward rapidity in p–Pb collisions at $\sqrt{s_{NN}} = 5.02$ TeV [59] to be larger than that in pp collisions at forward rapidity [19] but smaller than the ALICE measurements in pp and p–Pb collisions at midrapidity [5].

Recent attempts have been made to model charmed-baryon production in pp and p–Pb collisions. A framework based on a statistical hadronisation model [60], which takes into account an increased set of charmed-baryon states beyond those listed by the Particle Data Group (PDG), is able to reproduce the Λ_c^+/D^0 ratios measured by ALICE in the pp and p–Pb collision systems, although it overestimates the LHCb measurement in pp collisions. A model implementing hadronisation via recombination [61, 62], where the p_T distributions of light and charm quarks and antiquarks are inputs of the model and the relative production of single-charm baryons to single-charm mesons is treated as a free parameter, is able to reproduce the p_T dependence of the Λ_c^+/D^0 ratio measured by ALICE at central rapidity in pp and p–Pb collisions, and by LHCb at forward rapidity in p–Pb collisions. While models implementing different approaches to Λ_c^+ production are effective in describing the measured Λ_c^+/D^0 ratio and R_{pPb}, the large statistical and systematic uncertainties of the current measurements do not provide the discriminating power needed to differentiate between the various models. Therefore, more precise measurements are crucial in order to constrain predictions.

This paper presents the measurement of the p_T-differential production cross section of charmed Λ_c^+ baryons in pp collisions in the rapidity interval $|y| < 0.5$ and in p–Pb collisions in $-0.96 < y < 0.04$ at $\sqrt{s_{NN}} = 5.02$ TeV, performed with the ALICE detector at the LHC. The ratio of the production cross sections of Λ_c^+ baryons and D^0 mesons, Λ_c^+/D^0, and the nuclear modification factor R_{pPb} are also presented. Finally, the Λ_c^+ production cross section per unit of rapidity at midrapidity is computed by integrating the p_T-differential Λ_c^+ production cross section after extrapolating down to $p_T = 0$, and the p_T-integrated Λ_c^+/D^0 ratios are presented. Two hadronic decay channels of Λ_c^+ were studied: $\Lambda_c^+ \to pK^-\pi^+$ and $\Lambda_c^+ \to pK^0_S$. Different analysis strategies were implemented, taking advantage of the methods used in previous analyses for the hadronic decays of D mesons [63–68] and Λ_c^+ baryons [5]. With respect to our previous measurement of Λ_c^+ production [5], the p_T reach was extended, the overall uncertainties of the measurements were reduced, and the analysis was performed in finer p_T intervals. The precision of the measurement of the nuclear modification factor R_{pPb} was improved with respect to the previously published result thanks to the larger data samples as well as a pp reference measured at the same centre-of-mass energy.

The measurements are performed as the average of the particle and antiparticle cross sections, and so both Λ_c^+ and $\overline{\Lambda}_c^-$ baryons are referred to collectively as Λ_c^+ in the following. In all measurements the production cross section of prompt Λ_c^+ is reported, i.e. Λ_c^+ from direct hadronisation of a charm quark or from decays of directly produced excited charm states. For the centre-of-mass energy of pp collisions the simplified notation $\sqrt{s}$ is used throughout this paper.

It is noted that the Λ_c^+/D^0 baryon-to-meson ratio is the focus of a dedicated letter [69], and this document presents a more detailed description of the analysis procedure as well as supplementary results.

2 Experimental setup and data samples

The ALICE apparatus is composed of a central barrel, consisting of a set of detectors for particle reconstruction and identification covering the midrapidity region, a muon spectrometer at forward rapidity and various forward and backward detectors for triggering and event characterisation. The central barrel detectors cover the full azimuth in the pseudorapidity interval $|\eta| < 0.9$ and are embedded in a large solenoidal magnet that provides a $B = 0.5$ T field parallel to the beam direction (z-axis in the ALICE reference frame). A comprehensive description and overview of the typical performance of the detectors in pp and p–Pb collisions can be found in [70, 71].

The tracking and particle identification capabilities of the ALICE central barrel detectors were exploited to reconstruct the Λ_c^+ decay products at midrapidity. The Inner Tracking System (ITS), consisting of three subdetectors, the Silicon Pixel Detector (SPD), the Silicon Drift Detector (SDD), and the Silicon Strip Detector (SSD), each made of two concentric layers, allows for a precise determination of the track impact parameter (the distance of closest approach between the track and the primary vertex of the collision) in the transverse plane with a resolution better than 75 μm for tracks with $p_T > 1$ GeV/c [72]. The Time Projection Chamber (TPC) is the main tracking detector of the experiment [73]. It provides up to 159 space points to reconstruct the charged-particle trajectory, and provides charged-particle identification (PID) via the measurement of the specific energy loss dE/dx. The particle identification capabilities are extended by the Time-of-Flight (TOF) detector, which is used to measure the flight time of charged particles from the interaction point. The TOF detector is an array of Multi-gap Resistive Plate Chambers. It measures the particle arrival time at the detector with a resolution of about 80 ps. The start time of the collision is obtained for each event either using the TOF detector, the T0 detector, or a combination of the two [74]. The T0 detector consists of two arrays of Cherenkov counters, located on both sides of the interaction point, covering the pseudorapidity regions $4.61 < \eta < 4.92$ and $-3.28 < \eta < -2.97$, respectively. The time resolution of the T0 detector in pp and p–Pb collisions is about 50 ps for events in which a measurement is made on both sides of the interaction point [74]. The V0 detector system, used for triggering and event selection, consists of two scintillator arrays covering the full azimuth in the pseudorapidity intervals $2.8 < \eta < 5.1$ and $-3.7 < \eta < -1.7$ ([70], section 5.1). The Zero Degree Calorimeter (ZDC), used for offline event rejection in p–Pb collisions, consists of two sets of neutron and proton calorimeters positioned along the beam axis on both sides of the ALICE apparatus, about 110 m from the interaction point ([70], section 5.4).

The results presented in this paper were obtained from the analysis of the LHC Run 2 data samples collected from pp collisions at $\sqrt{s} = 5.02$ TeV in 2017 and p–Pb collisions at $\sqrt{s_{NN}} = 5.02$ TeV in 2016. The proton–nucleon centre-of-mass system in p–Pb collisions is shifted in rapidity by $\Delta y = 0.465$ in the direction of the proton beam (negative rapidity) due to the asymmetric beam energies of 4 TeV for protons and 1.59 TeV per nucleon for Pb nuclei. The analyses used events recorded with a minimum bias (MB) trigger, which was based on coincident signals from the V0 detectors in both pp and p–Pb collisions.

In order to remove background from beam–gas collisions and other machine-induced backgrounds, in pp collisions the events were further selected offline based on the correlation between the numbers of clusters and track segments reconstructed in the SPD, and V0 timing information. The latter was also used for the p–Pb analysis, together with the timing from the ZDC. In order to maintain a uniform ITS acceptance in pseudorapidity, only events with a z-coordinate of the reconstructed vertex position within 10 cm from the nominal interaction point were analysed. Events with multiple interaction vertices due to pileup from several collisions were removed using an algorithm based on tracks reconstructed with the TPC and ITS detectors [71]. Using these selection criteria, approximately one billion MB-triggered pp events were analysed, corresponding to an integrated luminosity of $\mathscr{L}_{\rm int}$ = 19.5 nb^{-1}($\pm$2.1% [75]), while approximately 600 million MB-triggered p–Pb events were selected, corresponding to $\mathscr{L}_{\rm int} = 287\ \mu$b^{-1} ($\pm$3.7% [76]).

3 Λ_c^+ analysis overview and methods

The analysis was performed using similar techniques to those reported in [5]. Λ_c^+ baryons were reconstructed in two hadronic decay channels: $\Lambda_c^+ \to \mathrm{pK}^-\pi^+$ (branching ratio, BR $= 6.28 \pm 0.33\%$), and $\Lambda_c^+ \to \mathrm{pK}^0_S$ (BR $= 1.59 \pm 0.08\%$), followed by the subsequent decay $\mathrm{K}^0_S \to \pi^+\pi^-$ (BR $= 69.2 \pm 0.05\%$) [77]. For the former, the Λ_c^+ decays to the $\mathrm{pK}^-\pi^+$ final state via four channels: $\Lambda_c^+ \to \mathrm{p}\overline{\mathrm{K}}^{*0}(892)$, $\Lambda_c^+ \to \Delta^{++}(1232)\mathrm{K}^-$, $\Lambda_c^+ \to \Lambda(1520)\pi^+$, and the non-resonant $\Lambda_c^+ \to \mathrm{pK}^-\pi^+$ decay. As these channels are indistinguishable in the analysis, all four are considered together.

The selection of candidates was performed using a combination of kinematical, geometrical, and PID selections. The selection criteria were tuned on Monte Carlo simulations in order to maximise the statistical significance in each $p_{\rm T}$ interval. Λ_c^+ candidates were reconstructed by combining reconstructed tracks with $|\eta| < 0.8$ and at least 70 reconstructed space points in the TPC. For all decay products in the $\Lambda_c^+ \to \mathrm{pK}^-\pi^+$ analysis and for the proton-candidate tracks in the $\Lambda_c^+ \to \mathrm{pK}^0_S$ analysis, at least one cluster was required in either of the two SPD layers. The PID selections for all analyses were performed utilising the Bayesian method for combining the TPC and TOF signals, as described in [78]. The Bayesian method entails the use of priors, an *a priori* probabilitiy of measuring a given particle species, which are determined using measured particle abundances. Where possible, the TPC and TOF signals were combined; however, if the TOF signal was absent for a given track, the TPC signal alone was used. For the $\Lambda_c^+ \to \mathrm{pK}^0_S$ analysis in p–Pb collisions, a machine learning approach with Boosted Decision Trees (BDTs) was also applied to select Λ_c^+ candidates, using the Toolkit for Multivariate Data Analysis (TMVA) [79].

The detector acceptance for Λ_c^+ baryons varies as a function of rapidity, in particular falling steeply to zero for $|y| > 0.5$ at low $p_{\rm T}$, and $|y| > 0.8$ for $p_{\rm T} > 5\,\mathrm{GeV}/c$. For this reason, a fiducial acceptance selection was applied on the rapidity of candidates, $|y_{\rm lab}| < y_{\rm fid}(p_{\rm T})$, where $y_{\rm fid}$ increases smoothly from 0.5 to 0.8 in $0 < p_{\rm T} < 5$ GeV$/c$ and $y_{\rm fid} = 0.8$ for $p_{\rm T} > 5\,\mathrm{GeV}/c$ [63].

For the $\Lambda_c^+ \to \mathrm{pK}^-\pi^+$ analysis, candidates were formed by combining triplets of tracks with the correct configuration of charge sign. For this decay channel, the high-resolution tracking and vertexing information provided by the ITS and TPC allows the interaction point (primary vertex) and the reconstructed decay point of the Λ_c^+ candidate (secondary vertex) to be distinguished from one another, despite the short decay length of the Λ_c^+ ($c\tau = 60.7\,\mu$m [77]). Once the secondary vertex was computed from the three tracks forming the Λ_c^+ candidate, selections were applied on variables related to the quality of the reconstructed vertex and the displaced decay vertex topology. These variables comprise the quadratic sum of the distance of closest approach of each track to the secondary vertex; the decay length of the Λ_c^+ candidate (separation between the primary and secondary vertices); the cosine of the pointing angle between the Λ_c^+ candidate flight line (the vector that connects the primary and secondary vertices), and the reconstructed momentum vector of the candidate. Selections were also applied on the transverse momenta of the decay products. Pions, kaons, and protons were identified using the *maximum-probability* Bayesian PID approach [78], where a probability is assigned to each track for every possible species based on the TPC and TOF signals and the identity of the track is taken to be the species with the highest probability value. This approach allows for a higher-purity sample to be selected, reducing the large level of combinatorial background and facilitating the signal extraction.

The $\Lambda_c^+ \rightarrow pK_S^0$ analysis started from a $K_S^0 \rightarrow \pi^+\pi^-$ candidate, which is reconstructed as a pair of opposite-sign charged tracks forming a neutral decay vertex displaced from the primary vertex (a V^0 candidate). This V^0 candidate was paired with a proton-candidate track originating from the primary vertex to form a Λ_c^+ candidate. Two strategies were then used to select Λ_c^+ candidates. The first, referred to in the following as 'standard' (STD), was based on rectangular selection criteria. The V^0 candidate was required to have an invariant mass compatible with the K_S^0 mass from the PDG [77] within 8 (20) MeV$/c^2$ at low (high) p_T, corresponding to one or two times the resolution of the K_S^0 invariant mass, depending on the p_T interval and the collision system. The V^0 candidates were selected based on the p_T and impact parameter of the decay pions to the K_S^0 decay vertex, and the cosine of the pointing angle between the V^0 flight line and its reconstructed momentum. Proton-candidate tracks were selected based on their p_T, their impact parameter to the primary vertex, the number of reconstructed TPC clusters, and a cluster being present on at least one of the two SPD layers. Particle identification was performed on the proton-candidate track, first using a loose $|n_\sigma| < 3$ pre-selection on the TPC response, where n_σ corresponds to the difference between the measured and expected dE/dx for a given particle species, in units of the resolution. This was followed by a strict requirement that the Bayesian posterior probability for the track to be a proton must be greater than 80%.

In p–Pb collisions, an approach using BDTs (also referred to as 'MVA' in the following) was used in addition to the STD analysis. The BDT algorithm provides a classification tree that maps simulated Λ_c^+ candidates to a single BDT response variable aiming to maximise the separation between signal and background candidates. The mapping function is then applied on a real data sample in which the true identities of particles are unknown, followed by the application of selections on the BDT response. Candidates were initially filtered using an $|{n_\sigma}^{TPC}| < 3$ PID selection on the proton candidate. Independent BDTs were trained for each p_T interval in the analysis. The training was performed on samples of simulated events including a detailed description of the experimental apparatus and the detector response. The training sample for signal candidates was taken from a simulation of pp events containing charmed hadrons generated using PYTHIA 6.4.25 [80] with the Perugia2011 tune [81], embedded into an underlying p–Pb collision generated with HIJING 1.36 [82]. The background candidates were taken from the HIJING simulation. The variables that were used in the training were the Bayesian PID probability of the proton-candidate track to be a proton, the p_T of the proton candidate, the invariant mass and $c\tau$ of the K_S^0 candidate, and the impact parameters of the V^0 and the proton-candidate track with respect to the primary vertex. The MC samples used for the efficiency calculation were different from those used in the training. The selection on the BDT response was tuned in each p_T interval to maximise the expected statistical significance, which is estimated using i) the signal obtained from the generated Λ_c^+ yield multiplied by the selection efficiency of the trained model and ii) the background estimated from preselected data multiplied by the background rejection factor from the BDT.

Signal extraction for all analyses was performed by means of a fit to the invariant mass distributions of candidates in each p_T interval under study. A Gaussian function was used to model the signal peak and an exponential function was used to model the background. Due to the small signal-to-background ratio, the standard deviation of the Gaussian signal function was fixed to the value obtained from simulations in order to improve the fit stability. In pp collisions, a Λ_c^+ signal could be extracted for the $\Lambda_c^+ \rightarrow pK^-\pi^+$ and $\Lambda_c^+ \rightarrow pK_S^0$ analyses in the range $1 < p_T < 12$ GeV. In p–Pb collisions a Λ_c^+ signal was extracted for the $\Lambda_c^+ \rightarrow pK_S^0$ analysis in the range $1 < p_T < 24$ GeV$/c$, and for the $\Lambda_c^+ \rightarrow pK^-\pi^+$ analysis in the range $2 < p_T < 24$ GeV$/c$, as the larger combinatorial background in the $\Lambda_c^+ \rightarrow pK^-\pi^+$ channel limits

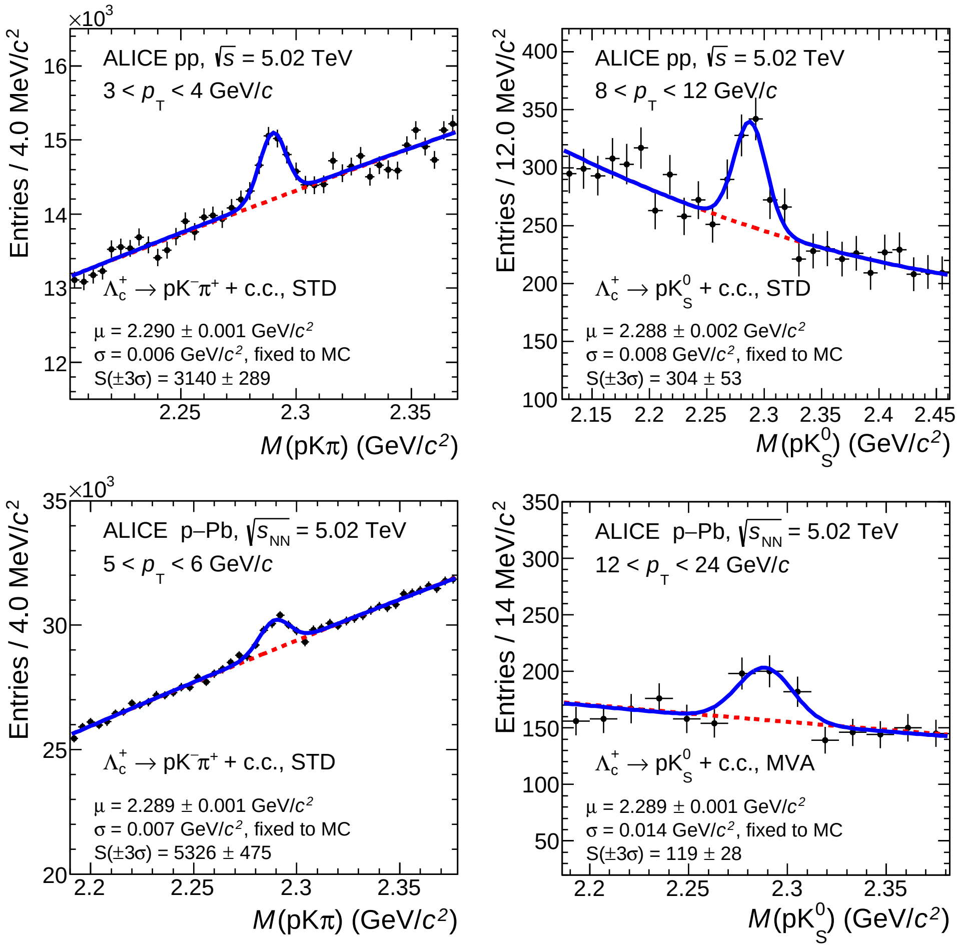

Figure 1: Invariant mass distributions of Λ_c^+ candidates in different p_T intervals, collision systems, and decay channels, with the corresponding fit functions. Top-left: $\Lambda_c^+ \to \mathrm{pK^-}\pi^+$ for $3 < p_T < 4$ GeV/c in pp collisions; top-right: $\Lambda_c^+ \to \mathrm{pK^0_S}$ for $8 < p_T < 12$ GeV/c in pp collisions; bottom-left: $\Lambda_c^+ \to \mathrm{pK^-}\pi^+$ for $5 < p_T < 6$ GeV/c with standard analysis in p–Pb collisions; bottom-right: $\Lambda_c^+ \to \mathrm{pK^0_S}$ with multivariate analysis in $12 < p_T < 24$ GeV/c in p–Pb collisions. The dashed lines represent the fit to the background and the solid lines represent the total fit function.

the low-p_T reach. A selection of the invariant mass distributions with their corresponding fit functions is displayed in Fig. 1 for different p_T intervals, decay channels, and collision systems.

4 Corrections

The p_T-differential cross section of prompt Λ_c^+-baryon production was obtained for each decay channel as

$$\frac{\mathrm{d}^2\sigma^{\Lambda_c^+}}{\mathrm{d}p_T\mathrm{d}y} = \frac{1}{2c_{\Delta y} \times \Delta p_T} \times \frac{1}{\mathrm{BR}} \times \frac{f_{\mathrm{prompt}} \times N^{\Lambda_c}_{|y|<y_{\mathrm{fid}}}}{(A \times \varepsilon)_{\mathrm{prompt}}} \times \frac{1}{\mathscr{L}_{\mathrm{int}}}, \tag{1}$$

where N^{Λ_c} is the raw yield (sum of particles and antiparticles) in a given p_T interval with width Δp_T, f_{prompt} is the fraction of the raw yield from prompt Λ_c^+, BR is the branching ratio for the considered decay mode, and $\mathscr{L}_{\mathrm{int}}$ is the integrated luminosity. $(A \times \varepsilon)$ is the product of detector acceptance and efficiency for prompt Λ_c^+ baryons, where ε accounts for the reconstruction of the collision vertex, the reconstruction and selection of the tracks of the Λ_c^+ decay products, and the Λ_c^+-candidate selection. The

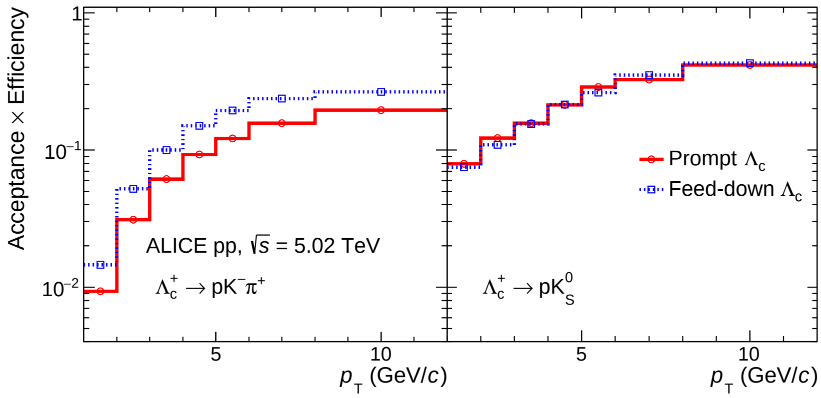

Figure 2: Product of detector acceptance and efficiency for Λ_c^+ baryons in pp collisions at $\sqrt{s} = 5.02$ TeV, as a function of p_T. From left to right: $\Lambda_c^+ \to pK^-\pi^+$ and $\Lambda_c^+ \to pK^0_S$. The solid lines correspond to the $(A \times \varepsilon)$ for prompt Λ_c^+, while the dotted lines represent $(A \times \varepsilon)$ for Λ_c^+ baryons originating from beauty-hadron decays. The statistical uncertainties are smaller than the marker size.

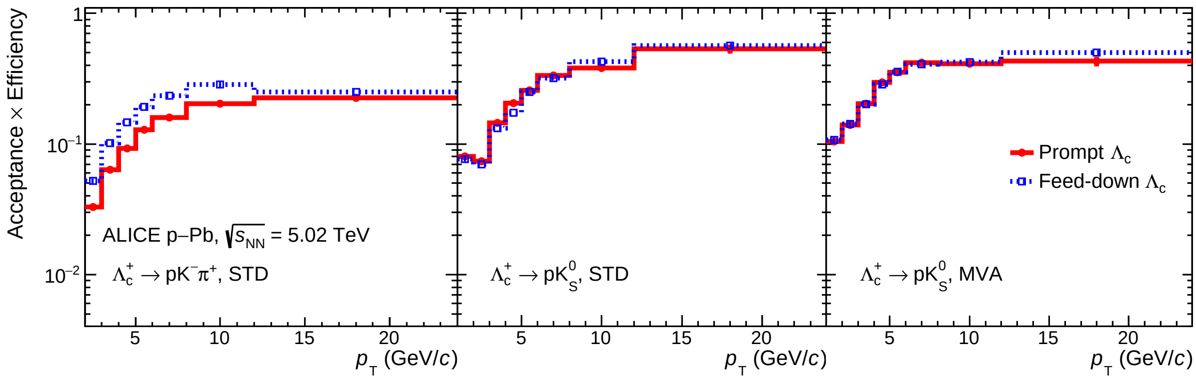

Figure 3: Product of detector acceptance and efficiency for Λ_c^+ baryons in p–Pb collisions at $\sqrt{s_{NN}} = 5.02$ TeV, as a function of p_T. From left to right: $\Lambda_c^+ \to pK^-\pi^+$, $\Lambda_c^+ \to pK^0_S$ with the STD technique, and $\Lambda_c^+ \to pK^0_S$ with the MVA technique. The solid lines correspond to the $(A \times \varepsilon)$ for prompt Λ_c^+, while the dotted lines represent $(A \times \varepsilon)$ for Λ_c^+ baryons originating from beauty-hadron decays. The statistical uncertainties are smaller than the marker size.

correction factor for the rapidity coverage, $c_{\Delta y}$, was computed as the ratio between the generated Λ_c^+-baryon yield in $|y_{lab}| < y_{fid}(p_T)$ and that in $|y_{lab}| < 0.5$. The factor 2 in the denominator of Eq. 1 takes into account that the raw yield includes both particles and antiparticles, while the cross section is given for particles only and is computed as the average of Λ_c^+ and $\overline{\Lambda}_c^-$.

The correction factor $(A \times \varepsilon)$ was obtained following the same approach as discussed in [66]. The correction factors were obtained from simulations in which the detector and data taking conditions of the corresponding data samples were reproduced. PYTHIA 6.4.25 and PYTHIA 8.243 [83] were used to simulate pp collisions. For p–Pb collisions, a pp event containing heavy-flavour signals was generated with PYTHIA 6 and HIJING was used to simulate the underlying background event.

The $(A \times \varepsilon)$ was computed separately for prompt and non-prompt Λ_c^+. The $\Lambda_c^+ \to pK^-\pi^+$ decay channel includes not only the direct (non-resonant) decay mode, but also three resonant channels, as explained in Section 3. Due to the kinematical properties of these decays, the acceptance and efficiency of each decay mode is different and the final correction was determined as a weighted average of the $(A \times \varepsilon)$ values of the four decay channels with the relative branching ratios as weights.

Figures 2 and 3 show the product of $(A \times \varepsilon)$ for Λ_c^+ baryons with $|y| < y_{fid}$ in pp and p–Pb collisions as a function of p_T for the $\Lambda_c^+ \to pK^-\pi^+$ (left panel) and $\Lambda_c^+ \to pK_S^0$ (middle and right panels) decay channels. The higher $(A\times\varepsilon)$ for Λ_c^+ from beauty-hadron decays in the $\Lambda_c^+ \to pK^-\pi^+$ decay channel is due to the geometrical selections on the displaced decay-vertex topology, which enhance the non-prompt component because of the relatively longer lifetime of the beauty hadrons compared to prompt Λ_c^+. For the $\Lambda_c^+ \to pK_S^0$ analyses, the $(A\times\varepsilon)$ of prompt and non-prompt Λ_c^+ are compatible, as selections based on the displaced decay-vertex topology are not applied. The $(A\times\varepsilon)$ of the MVA analysis is on average around 50% higher than that of the STD analysis at low p_T, meaning that a more efficient selection on Λ_c^+ decays is achieved with the MVA approach.

Unlike the case of pp collisions, where the charged-particle multiplicity in data is well described by the simulation, in p–Pb collisions a weighting procedure based on the event multiplicity was used in the calculation of the reconstruction efficiency from the simulated events. This approach accounts for the dependence of the reconstruction efficiency on the event multiplicity, which is due to the fact that the resolutions of the primary-vertex position and of the variables used in the geometrical selections of displaced decay vertices improve with increasing multiplicity. The event multiplicity was defined here using the number of tracklets, where a tracklet is defined as a track segment joining the reconstructed primary vertex with a space point on each SPD layer within the pseudorapidity range $|\eta| < 1.0$.

The factor $f_{\rm prompt}$ was calculated as

$$f_{\rm prompt} = 1 - \frac{N^{\Lambda_c \text{feed-down}}}{N^{\Lambda_c}} = 1 - \frac{(A\times\varepsilon)_{\text{feed-down}}\, c_{\Delta y}\, \Delta p_T\, \text{BR}\, \mathscr{L}_{\rm int}}{N^{\Lambda_c}/2} \times \left(\frac{\mathrm{d}^2\sigma}{\mathrm{d}p_T\mathrm{d}y}\right)^{\rm FONLL}_{\text{feed-down}}, \quad (2)$$

where $N^{\Lambda_c}/2$ is the raw yield divided by a factor of two to account for particles and antiparticles. The production cross section of Λ_c^+ from Λ_b^0-baryon decays, $\left(\frac{\mathrm{d}^2\sigma}{\mathrm{d}p_T\mathrm{d}y}\right)^{\rm FONLL}_{\rm feed-down}$, was calculated using the b-quark p_T-differential cross section from FONLL calculations [3, 4], the fraction of beauty quarks that fragment into Λ_b^0 estimated from LHCb measurements [23], and the $\Lambda_b^0 \to \Lambda_c^+ + X$ decay kinematics modelled using PYTHIA 8 simulations [83], normalised according to the branching ratio $f(\Lambda_b^0 \to \Lambda_c^+ + \mathrm{X}) = 33\%$ [77].

The $\mathrm{b} \to \Lambda_b^0$ fragmentation was derived from the LHCb measurements of Λ_b^0-production fraction relative to $\overline{\mathrm{B}}^0$ and B^- mesons in pp collisions at $\sqrt{s} = 13$ TeV [23], which indicates that the fraction of b quarks hadronising into a Λ_b^0 baryon is strongly p_T-dependent in the measured range of $4 < p_T < 25$ GeV/c. The fits to the production fractions of $\overline{\mathrm{B}}_s^0$ and Λ_b^0 hadrons normalised to the sum of B^- and $\overline{\mathrm{B}}^0$ hadrons are presented in [23] as a function of the beauty-hadron p_T as

$$\frac{f_s}{f_u+f_d}(p_T) = A[p_1 + p_2 \times (p_T - <p_T>)] = X, \quad (3)$$

$$\frac{f_{\Lambda_b^0}}{f_u+f_d}(p_T) = C[q_1 + \exp(q_2 + q_3 \times p_T)] = Y, \quad (4)$$

where f_u, f_d, f_s, and $f_{\Lambda_b^0}$ are the fractions of b quarks that hadronise into $\overline{\mathrm{B}}^0$, B^-, $\overline{\mathrm{B}}_s^0$, and Λ_b^0, respectively, and A, p_1, p_2, $<p_T>$, C, q_1, q_2 and q_3 are free parameters of the fits to the measured ratios. Assuming $f_u = f_d$ and $f_u + f_d + f_s + f_{\Lambda_b^0} = 1$ the Λ_b^0 fragmentation fraction can be defined as

$$f_{\Lambda_b^0}(p_T) = \frac{Y}{(X+Y+1)}. \quad (5)$$

For $p_T = 5$ GeV/c, $f_{\Lambda_b^0}$ is around 0.2, and it decreases to a value of around 0.09 for $p_T > 20$ GeV/c. For $p_T < 5$ GeV/c it was assumed that $f_{\Lambda_b^0} = 0.2$, since measurements of the ratio $\Lambda_b^0/\overline{\mathrm{B}}^0$ in pp collisions at $\sqrt{s} = 7$ TeV and 8 TeV [22] are flat as a function of p_T in this interval within the experimental uncertainties. It was assumed that there is no rapidity dependence of $f_{\Lambda_b^0}$ since the LHCb measurements of beauty-production ratios are flat as a function of rapidity in $2 < y < 5$ within the experimental uncertainties [22, 23].

For p–Pb collisions, a hypothesis on the nuclear modification factor $R_{pPb}^{\text{feed-down}}$ of Λ_c^+ from beauty-hadron decays was included as an additional factor in the last term of Eq. 2. As in the D-meson analyses [64], it was assumed that the R_{pPb} of prompt and feed-down Λ_c^+ are equal. The values of f_{prompt} in both collision systems range between 92% and 99% for the $\Lambda_c^+ \to pK_S^0$ decay channel and between 89% and 99% for the $\Lambda_c^+ \to pK^-\pi^+$ decay channel.

5 Evaluation of systematic uncertainties

This section describes the various sources of systematic uncertainties in each analysis, and the methods used to estimate them. A summary of the systematic uncertainties is shown in Tab. 1 and Tab. 2 for the pp and p–Pb analyses, respectively. The different sources of systematic uncertainty are assumed to be uncorrelated, and their contributions are added in quadrature to calculate the overall systematic uncertainty in each p_T interval.

The systematic uncertainty on the yield extraction was estimated by repeating the fits to the invariant mass distributions several times, varying i) the lower and upper limits of the fit interval, and ii) the functional form of the background (linear, exponential, and second-order polynomial functions were used). For each of the above trials, the fit was repeated with different hypotheses on the signal peak width and mean, with variations including a) treating both the Gaussian width and mean as free parameters, b) fixing the peak width to the MC expectation and leaving the mean free, c) fixing the mean to the MC expectation and leaving the peak width free, and d) fixing both the peak width and mean to the MC expectation. The systematic uncertainty was defined as the RMS of the distribution of the raw yield values extracted from these trials.

The systematic uncertainty on the tracking efficiency was estimated by i) comparing the probability of prolonging a track from the TPC to the ITS (“matching efficiency”) in data and simulation, and ii) by varying track selection criteria in the analyses. The matching efficiency in simulation was determined after re-weighting the relative abundance of primary and secondary particles to match that in data. The uncertainty on the matching efficiency was defined as the relative difference in the matching efficiency between simulation and data. It is species-dependent and therefore it was determined individually for protons, kaons, and pions. In the $\Lambda_c^+ \to pK_S^0$ analysis only the proton matching efficiency uncertainty was included since no ITS condition was required for the pion tracks from the K_S^0 decay. The per-track uncertainty on the matching efficiency is p_T dependent and it was propagated to the Λ_c^+ taking into account the decay kinematics and treating the uncertainty as correlated among the tracks. The second contribution to the track reconstruction uncertainty was estimated by repeating the analysis varying the TPC track selection criteria. The uncertainty was defined as the RMS of the Λ_c^+ cross section values obtained with the different track selections. The total uncertainty on the tracking efficiency was defined as the quadratic sum of these two contributions.

The uncertainty on the Λ_c^+ selection efficiency due to imperfections in the simulated kinematical and geometrical variables used to select Λ_c^+ candidates was estimated by varying the selection criteria. For the MVA analysis in the $\Lambda_c^+ \to pK_S^0$ channel, variations were made on the selection of the BDT response. The systematic uncertainty was estimated in each p_T interval as the RMS of the distribution of the corrected cross section values resulting from these variations.

Systematic uncertainties can arise from discrepancies in the PID efficiency between simulation and data. In the case of the $\Lambda_c^+ \to pK_S^0$ analysis, the systematic uncertainty associated with the PID efficiency was estimated by varying the minimum probability threshold required to identify a track as a proton. For the $\Lambda_c^+ \to pK^-\pi^+$ analysis, the systematic uncertainty was estimated by applying a minimum threshold selection on the Bayesian probability to assign the track identity, with the threshold varying between 30% and 80%. The systematic uncertainty in both cases was defined based on the variation of the corrected cross section. For the MVA analysis, the PID variables were included as part of the BDT, and therefore the PID uncertainty is already accounted for by varying the selection on the BDT response. The contribution due to the 3σ PID preselection was found to be negligible.

An additional source of systematic uncertainty was assigned due to the dependence of the efficiencies on the generated p_T distribution of Λ_c^+ in the simulation. To estimate this effect the efficiencies were evaluated after reweighting the p_T shape of the PYTHIA 6 simulations to match the p_T spectrum of D mesons from FONLL pQCD calculations. An uncertainty was assigned in each p_T interval based on the difference between the central and reweighted efficiencies.

The relative statistical uncertainty on $(A \times \varepsilon)$ was considered as an additional systematic uncertainty source, originating from the finite statistics in the simulation used to calculate the efficiency.

The systematic uncertainty on the prompt fraction was estimated by varying independently i) the production cross section of beauty quarks within the theoretical uncertainties in FONLL [4], and ii) the function describing the fragmentation fraction $f_{\Lambda_b^0}$. For the variation of ii), the free parameters defined in [23] were varied independently within their uncertainties. For $p_T(\Lambda_b^0) < 5$ GeV/c, the lower uncertainty bound of $f_{\Lambda_b^0}$ was taken to be equal to the lower bound of the fit at $p_T(\Lambda_b^0) = 5$ GeV/c, independent of p_T, while the upper uncertainty bound was taken to be equal to the p_T-dependent upper bound of the fit. In order to account for a possible $\sqrt{s}$ dependence of the fragmentation fractions, an additional reduction of the lower bound of $f_{\Lambda_b^0}$ was considered based on the spread of the LHCb measurements at different values of $\sqrt{s}$. In the p–Pb analyses the uncertainty on the hypothesis of the nuclear modification factor of Λ_c^+ from beauty-hadron decays was estimated by varying the ratio $R_{\rm pPb}^{\rm feed\text{-}down}/R_{\rm pPb}^{\rm prompt}$ in the range $0.9 < R_{\rm pPb}^{\rm feed\text{-}down}/R_{\rm pPb}^{\rm prompt} < 1.3$. This range was chosen based on theoretical calculations of charm and beauty hadron production in p–Pb collisions as explained in [64]. The overall uncertainty on the prompt fraction was defined as the envelope of these variations, which leads to an asymmetric uncertainty.

The uncertainty on the luminosity measurement is 2.1% for pp collisions [75] and 3.7% for p–Pb collisions [76]. The uncertainty on the branching fractions are 5.1% for the $\Lambda_c^+ \to pK^-\pi^+$ channel, and 5.0% for the $\Lambda_c^+ \to pK_S^0$ channel [77].

	$\Lambda_c^+ \to pK^-\pi^+$		$\Lambda_c^+ \to pK^0_S$	
	lowest p_T	highest p_T	lowest p_T	highest p_T
Yield extraction (%)	10	8	8	7
Tracking efficiency (%)	6	7	3	5
Selection efficiency (%)	6	6	3	3
PID efficiency (%)	5	5	2	4
MC p_T shape (%)	negl.	negl.	negl.	negl.
$(A \times \varepsilon)$ stat. unc. (%)	1.7	2.6	1.6	3.7
Beauty feed-down (%)	$^{+0.6}_{-0.8}$	$^{+3.7}_{-4.4}$	$^{+0.6}_{-0.8}$	$^{+2.3}_{-2.6}$
Branching ratio (%)	5.1		5.0	
Luminosity (%)	2.1			

Table 1: Summary of the systematic uncertainties for the two Λ_c^+ decay modes in pp collisions at $\sqrt{s} = 5.02$ TeV. The uncertainty sources found to be $< 1\%$ were considered negligible ("negl." in the table).

	$\Lambda_c^+ \to pK^-\pi^+$ (STD)		$\Lambda_c^+ \to pK^0_S$ (STD)		$\Lambda_c^+ \to pK^0_S$ (MVA)	
	lowest p_T	highest p_T	lowest p_T	highest p_T	lowest p_T	highest p_T
Yield extraction (%)	8	10	11	8	10	8
Tracking efficiency (%)	6	6	6	5	6	5
Selection efficiency (%)	10	6	4	4	15	8
PID efficiency (%)	5	5	3	3	negl.	negl.
MC p_T shape (%)	1	1	1	1	1	1
$(A \times \varepsilon)$ stat. unc. (%)	1.2	5.4	0.6	3.1	0.5	2.9
Beauty feed-down (%)	$^{+1.0}_{-1.3}$	$^{+1.7}_{-2.6}$	$^{+0.6}_{-0.9}$	$^{+2.4}_{-3.6}$	$^{+0.7}_{-0.9}$	$^{+2.7}_{-3.9}$
Branching ratio (%)	5.1		5.0			
Luminosity (%)	3.7					

Table 2: Summary of the systematic uncertainties for the two Λ_c^+ decay modes in p–Pb collisions at $\sqrt{s_{NN}} = 5.02$ TeV. For the $\Lambda_c^+ \to pK^0_S$ analyses, the two analysis methods described in the text are quoted separately. The uncertainty sources found to be $< 1\%$ were considered negligible ("negl." in the table).

6 Results

6.1 p_T-differential cross sections

The p_T-differential cross section of prompt Λ_c^+-baryon production in pp collisions at $\sqrt{s} = 5.02$ TeV, measured in the rapidity interval $|y| < 0.5$ and p_T interval $1 < p_T < 12$ GeV/c, is shown in Fig. 4 (left) for the two decay channels $\Lambda_c^+ \to pK^-\pi^+$ and $\Lambda_c^+ \to pK^0_S$. Figure 4 (right) shows the p_T-differential cross section of prompt Λ_c^+-baryon production in p–Pb collisions at $\sqrt{s_{NN}} = 5.02$ TeV, measured in the rapidity interval $-0.96 < y < 0.04$ and p_T interval $1 < p_T < 24$ GeV/c for the two decay channels $\Lambda_c^+ \to pK^-\pi^+$ and $\Lambda_c^+ \to pK^0_S$ and the two different analysis techniques. The measurements in the different decay channels agree within statistical and uncorrelated systematic uncertainties, with the largest discrepancies among the measured values being smaller than 2.2σ.

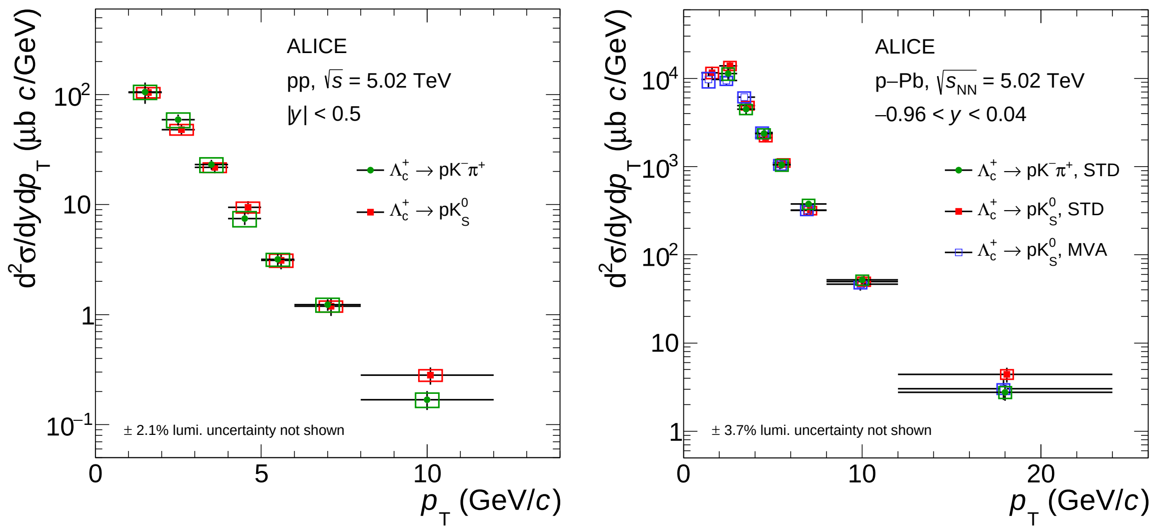

Figure 4: Left: p_T-differential prompt Λ_c^+-baryon cross section in pp collisions at $\sqrt{s} = 5.02$ TeV in the interval $1 < p_T < 12$ GeV/c. Right: p_T-differential prompt Λ_c^+-baryon cross section in p–Pb collisions at $\sqrt{s_{NN}} = 5.02$ TeV in the interval $1 < p_T < 24$ GeV/c. The results for the two different decay channels and the two different analysis techniques are shown in the figure. The statistical uncertainties are shown as vertical bars and the systematic uncertainties are shown as boxes. Horizontal position of points are shifted to provide better visibility.

To obtain a more precise measurement of the p_T-differential Λ_c^+-baryon production cross section, the results from the two decay channels and the two analysis techniques were combined, taking into account the correlation between the statistical and systematic uncertainties. The systematic uncertainties treated as uncorrelated between the different decay channels ($\Lambda_c^+ \to pK^-\pi^+$ and $\Lambda_c^+ \to pK^0_S$) include those due to the raw-yield extraction, the Λ_c^+-selection efficiency, and the $(A \times \varepsilon)$ statistical uncertainties. The systematic uncertainties due to the tracking efficiency, the PID efficiency, the generated Λ_c^+ p_T spectrum, the beauty feed-down, and the luminosity were treated as correlated between the two decay channels. The branching ratio uncertainties were considered to be partially correlated, as described in [77]. A weighted average of the cross section values obtained from the different analyses was calculated, using the inverse of the quadratic sum of the relative statistical and uncorrelated systematic uncertainties as weights. In the case of p–Pb collisions, the results of the $\Lambda_c^+ \to pK^0_S$ analysis obtained with the STD and MVA methods were averaged before combining the different decay channels. The statistical uncertainties in this merging step were considered to be fully correlated between the STD and MVA results, the systematic uncertainties due to the raw-yield extraction were considered to be uncorrelated, and all other systematic uncertainty sources were considered to be fully correlated. The weighted average of the STD and MVA results for the $\Lambda_c^+ \to pK^0_S$ cross section was calculated using the inverse of the squared relative uncorrelated systematic uncertainties as weights. The result was then averaged with the $\Lambda_c^+ \to pK^-\pi^+$

cross section following the same method used for pp collisions.

Figure 5 shows the measured production cross section (average of the two decay channels) in pp collisions compared to predictions from MC generators and pQCD calculations. The left panel shows the comparison with predictions from different tunes of the PYTHIA 8 generator, including the Monash tune [13], and tunes that implement colour reconnection (CR) beyond the leading-colour approximation [14]. These additional colour reconnection topologies include 'junctions' which fragment into baryons, leading to increased baryon production. For the CR tunes, three modes are considered (Mode 0, 2, and 3), as described in [14], which apply different constraints on the allowed reconnection, taking into account causal connection of dipoles involved in a reconnection and time-dilation effects caused by relative boosts between string pieces. It is noted that Mode 2 is recommended in [14] as the standard tune, and contains the strictest constraints on the allowed reconnection. In the simulations with the three CR modes, all soft QCD processes are switched on. All PYTHIA 8 tunes underestimate the measured p_T-differential prompt Λ_c^+ cross section. The Monash tune significantly underestimates the cross section by a factor $\sim$15 for $1 < p_T < 2$ GeV/c, and around a factor 2–3 for $p_T > 8$ GeV/c. All three CR modes yield a similar magnitude and shape of the Λ_c^+ cross section, and predict a significantly larger Λ_c^+ production cross section with respect to the Monash tune. However, for all three CR modes, the measured Λ_c^+ production cross section is underestimated by a factor of about two for $1 < p_T < 2$ GeV/c. For $p_T > 5$ GeV/c, the measured Λ_c^+-production cross section is underestimated by 15–40% depending on the CR mode. All tunes exhibit a harder p_T distribution than observed in data.

The right panel of Fig. 5 shows a comparison with a NLO pQCD calculation obtained with the POWHEG framework [84], matched with PYTHIA 6 to generate the parton shower, and the CT14NLO parton distribution functions [85]. The nominal factorisation and renormalisation scales, μ_F and μ_R, were taken to be equal to the transverse mass of the quark, $\mu_0 = \sqrt{m^2 + p_T^2}$, and the charm-quark mass was set to $m_c = 1.5$ GeV/c^2. The theoretical uncertainties were estimated by varying these scales in the range $0.5\mu_0 < \mu_{R,F} < 2.0\mu_0$, with $0.5\mu_0 < \mu_R/\mu_F < 2.0\mu_0$. Results are also compared with recent GM-VFNS pQCD calculations [86]. With respect to previous GM-VFNS calculations [1, 2], a new fragmentation function for Λ_c^+ has been used, obtained from a fit to OPAL data [87] and measurements from Belle at $\sqrt{s}$ = 10.52 GeV [88]. The measured p_T-differential cross section is significantly underestimated by the POWHEG prediction, by a factor of up to 20 in the lowest p_T interval of the measurements, and around a factor 3 in the highest. While the discrepancy between the data and calculation decreases as the p_T increases, the measured cross section at $8 < p_T < 12$ GeV/c is still $\sim$50% larger than the upper edge of the POWHEG uncertainty band. The discrepancy between the data and POWHEG is similar to what was observed in pp collisions at $\sqrt{s} = 7$ TeV [5]. The GM-VFNS predictions also significantly underestimate the data, by about a factor of 3–4 at low p_T and by about a factor of 2 at high p_T.

In Fig. 6, the Λ_c^+-production cross section in pp collisions at $\sqrt{s} = 5.02$ TeV is compared with the measurement at $\sqrt{s} = 7$ TeV [5]. For a direct comparison, the intervals $4 < p_T < 5$ GeV/c and $5 < p_T < 6$ GeV/c of the $\sqrt{s} = 5.02$ TeV analysis have been merged. When merging, the systematic uncertainties were propagated considering the uncertainty due to the raw-yield extraction as fully uncorrelated and all the other sources as fully correlated between p_T intervals. In the lower panel of the same figure, the ratio of the cross sections is shown. In this case, the systematic uncertainties on feed-down, p_T shape, and branching ratio were assumed to be fully correlated, while all the other sources were considered as uncorrelated between the results at the two collision energies. The relative statistical uncertainties in the measurement at $\sqrt{s} = 5.02$ TeV are on average smaller than those in the measurement at $\sqrt{s} = 7$ TeV by a factor $\sim$1.5. As expected, a lower Λ_c^+-production cross section is observed at the lower collision energy. The difference between the cross sections at the two $\sqrt{s}$ values increases with increasing p_T, indicating a harder p_T shape at the higher collision energy. This behaviour is consistent with that observed for the D-meson cross section ratios at $\sqrt{s} = 7$ TeV and $\sqrt{s} = 5.02$ TeV, which is described by pQCD calculations [89].

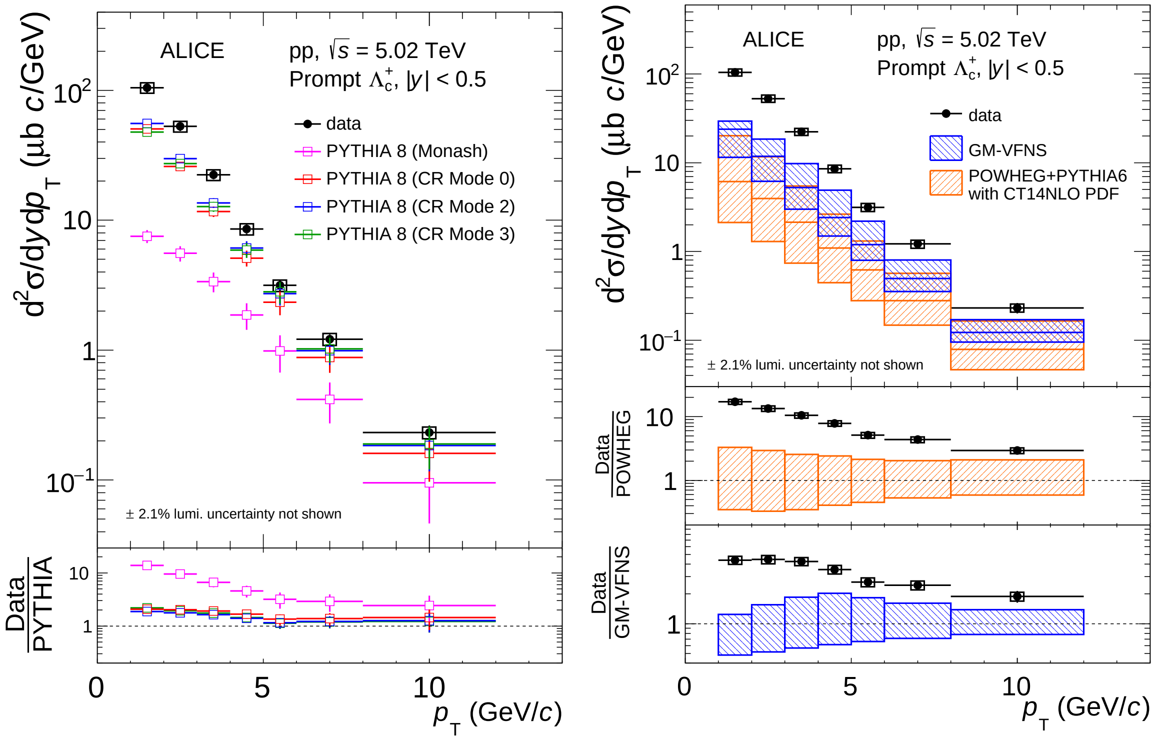

Figure 5: Prompt Λ_c^+-baryon p_T-differential production cross section in pp collisions at $\sqrt{s} = 5.02$ TeV in the interval $1 < p_T < 12$ GeV$/c$. The statistical uncertainties are shown as vertical bars and the systematic uncertainties are shown as boxes. Left: Comparison to predictions from different tunes of the PYTHIA 8 event generator [13] [14]. The vertical bars on the PYTHIA 8 predictions represent the statistical uncertainty from the simulation, and the vertical bars on the ratios in the bottom panel also include the statistical uncertainties from the data. Right: Comparison to predictions from the POWHEG event generator [84] and GM-VFNS calculations [86]. The orange(blue) boxes represent the uncertainties of POWHEG(GM-VFNS) due to the choice of pQCD scales. See text for details on the PYTHIA 8 and POWHEG event generator settings.

Figure 7 shows the p_T-differential cross section averaged among the decay channels and analysis techniques in p–Pb collisions. The cross section is compared to the POWHEG event generator, where the generator settings, the parton shower, and the set of parton distribution functions are the same as used in the calculations for pp collisions, and the nuclear modification of the parton distribution functions is modelled with the EPPS16 nPDF parameterisation [38]. The theoretical uncertainty includes the uncertainty on the factorisation and renormalisation scales (estimated as done for POWHEG predictions for pp collisions), while the uncertainties on the parton distribution functions and EPPS16 nPDF are not included in the calculation as they are smaller than the scale uncertainties. The cross section is underestimated by the POWHEG prediction by a factor of up to 20 in the lowest p_T interval, similar to what is observed for pp collisions. The difference between the POWHEG predictions and the measured cross section decreases with increasing p_T and in the highest p_T interval of the measurement ($12 < p_T < 24$ GeV$/c$) the data point lies on the upper edge of the POWHEG uncertainty band. The Run 2 p–Pb results are compatible with our previous results from the sample of p–Pb collisions at $\sqrt{s_{NN}} = 5.02$ TeV collected in LHC Run 1 [5]. The statistical uncertainties have been reduced by approximately a factor of two for all p_T intervals, and the systematic uncertainties improved by approximately 30% at low p_T and 10% at high p_T.

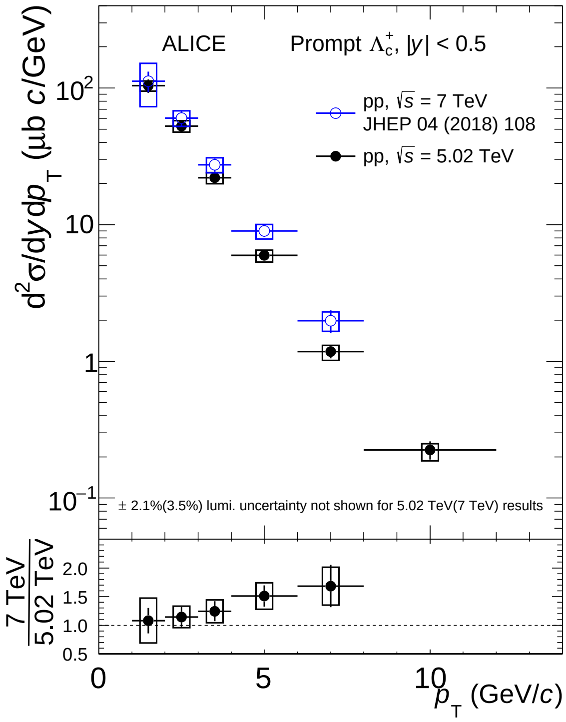

Figure 6: Comparison between the p_T-differential production cross section of prompt Λ_c^+ baryons in pp collisions at $\sqrt{s} = 7$ TeV [5] and $\sqrt{s} = 5.02$ TeV. The ratio between the cross sections is shown in the lower panel. The statistical uncertainties are shown as vertical bars and the systematic uncertainties are shown as boxes.

6.2 Nuclear modification factor

The nuclear modification factor R_{pPb} was calculated as the p_T-differential Λ_c^+ cross section in p–Pb collisions divided by the reference measurement of the p_T-differential Λ_c^+ cross section in pp collisions scaled by the lead mass number $A = 208$

$$R_{pPb} = \frac{1}{A} \frac{d\sigma_{pPb}/dp_T}{d\sigma_{pp}/dp_T} \tag{6}$$

where $d\sigma_{pp}/dp_T$ was obtained from the cross section measured in pp collisions in $|y| < 0.5$ applying a correction factor to account for the different rapidity coverage of the pp and p–Pb measurements. The correction factor is calculated with FONLL and ranges from 0.995 (in $1 < p_T < 2$ GeV$/c$) to 0.983 (in $8 < p_T < 12$ GeV$/c$). Figure 8 (left) shows the R_{pPb} of Λ_c^+ baryons in the p_T interval $1 < p_T < 12$ GeV$/c$ compared to the R_{pPb} of non-strange D mesons from [90]. With respect to the previous measurement of the Λ_c^+-baryon R_{pPb} [5], the p_T reach has been extended to higher and lower p_T. In addition, the pp reference at the same per-nucleon centre-of-mass energy as the p–Pb sample eliminates the uncertainty originating from the $\sqrt{s}$-scaling of the pp cross section measured at $\sqrt{s} = 7$ TeV that was present in the previous results. These improvements, along with the increased statistical precision, have allowed for a reduction of the overall uncertainty of the R_{pPb} by a factor of 1.7–2 compared with the previous measurement. The result is consistent with the D-meson R_{pPb} within the uncertainties. For $p_T > 2$ GeV$/c$ the Λ_c^+-baryon R_{pPb} is consistent with unity, although the central values of the data points are systematically above unity. In the p_T interval $1 < p_T < 2$ GeV$/c$ the R_{pPb} is lower than unity by 4.1σ, where σ is defined as the quadratic sum of the statistical and the upper systematic uncertainty. This suggests that Λ_c^+ production at low p_T is suppressed in p–Pb collisions with respect to pp collisions. In Fig. 8 (right) the measured Λ_c^+-baryon R_{pPb} is compared to model calculations. The POWHEG+PYTHIA 6 simulations

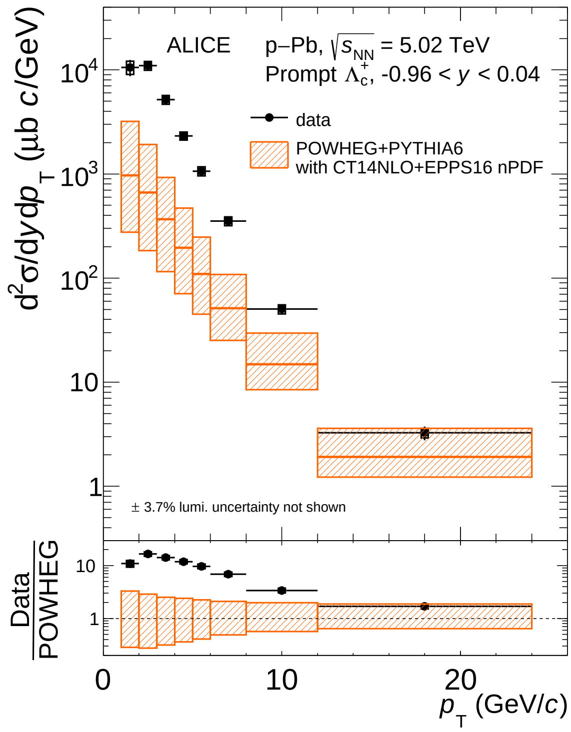

Figure 7: p_T-differential prompt Λ_c^+-baryon production cross section in p–Pb collisions at $\sqrt{s_{NN}} = 5.02$ TeV in the interval $1 < p_T < 24$ GeV/c compared to predictions from the POWHEG event generator [84]. The statistical uncertainties are shown as vertical bars and the systematic uncertainties are shown as boxes. The orange boxes represent the uncertainties of POWHEG due to the choice of pQCD scales. See text for details on the POWHEG event generator settings.

use the POWHEG event generator with PYTHIA 6 parton shower and EPPS16 parameterisation of the nuclear modification of the PDFs [38]. The uncertainty band includes the uncertainties on the nuclear PDFs and on the choice of the pQCD scales. The POWLANG model [58] assumes that a hot deconfined medium is formed in p–Pb collisions, and the transport of heavy quarks through an expanding QGP is computed utilising the Langevin approach and Hard Thermal Loop (HTL) transport coefficients. The POWLANG model does not implement specific differences in hadronisation mechanisms for baryons and mesons, and the same prediction holds for all charmed hadron species. The two models capture some features of the data, but neither of them can quantitatively reproduce the observed Λ_c^+-baryon R_{pPb} in the measured p_T interval.

6.3 p_T-integrated Λ_c^+ cross sections

The visible Λ_c^+ cross section was computed by integrating the p_T-differential cross section in its measured range. In the integration, the systematic uncertainties were propagated considering the uncertainty due to the raw-yield extraction as fully uncorrelated and all the other sources as fully correlated between p_T intervals. The visible Λ_c^+ cross section in pp collisions at $\sqrt{s} = 5.02$ TeV is

$$d\sigma^{\Lambda_c^+}_{pp,\ 5.02\ \mathrm{TeV}}/dy|^{1<p_T<12\ \mathrm{GeV}/c}_{|y|<0.5} = 195 \pm 11\ (\mathrm{stat.}) \pm 17\ (\mathrm{syst.}) \pm 4\ (\mathrm{lumi.})\mu\mathrm{b}. \quad (7)$$

The visible Λ_c^+ cross section in p–Pb collisions is

$$d\sigma^{\Lambda_c^+}_{pPb,\ 5.02\ \mathrm{TeV}}/dy|^{1<p_T<24\ \mathrm{GeV}/c}_{-0.96<y<0.04} = 31.1 \pm 2.1\ (\mathrm{stat.}) \pm 3.3\ (\mathrm{syst.}) \pm 1.1\ (\mathrm{lumi.})\ \mathrm{mb}. \quad (8)$$

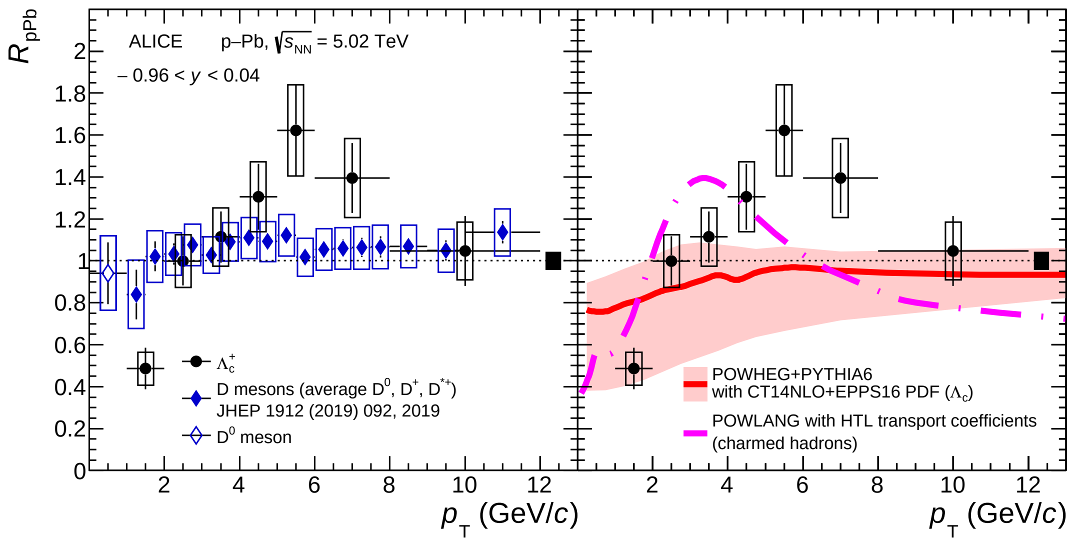

Figure 8: The nuclear modification factor R_{pPb} of prompt Λ_c^+ baryons in p–Pb collisions at $\sqrt{s_{NN}} = 5.02$ TeV as a function of p_T, compared to the R_{pPb} of D mesons [90] (average of D^0, D^+, and D^{*+} in the range $1 < p_T < 12$ GeV/c and D^0 in $0 < p_T < 1$ GeV/c) (left), as well as to POWHEG+PYTHIA 6 [84] with EPPS16 [38] simulations, and POWLANG [58] predictions (right). The black-filled box at $R_{pPb} = 1$ represents the normalisation uncertainty.

The p_T-integrated Λ_c^+ production cross section at midrapidity was obtained by extrapolating the visible cross sections to the full p_T range. The extrapolation approach used for D mesons [63], based on the p_T-differential cross sections predicted by FONLL calculations, is not applicable here because FONLL does not have predictions for Λ_c^+ baryons. For pp collisions, PYTHIA 8 predictions with specific tunes implementing CR mechanisms were used for the extrapolation. The p_T-differential Λ_c^+ cross section values in $0 < p_T < 1$ GeV/c and for $p_T \geq 12$ GeV/c were obtained by scaling the measured Λ_c^+ cross section in $1 < p_T < 12$ GeV/c for the fractions of cross section given by PYTHIA in $0 < p_T < 1$ GeV/c and for $p_T \geq 12$ GeV/c respectively. The PYTHIA 8 simulation with Mode 2 CR tune [14] including soft QCD processes, which gives the best description of both the magnitude and shape of the Λ_c^+ cross section and Λ_c^+/D^0 ratio, was used to calculate the central value of the extrapolation factors. The procedure was repeated considering the three modes defined in [14], with the envelopes of the corresponding results assigned as the extrapolation uncertainty. A second extrapolation method was also implemented as a cross check. This consisted of multiplying the measured D^0 cross section value in $0 < p_T < 1$ GeV/c by the Λ_c^+/D^0 ratio estimated with PYTHIA 8 (CR Mode 2) in the same p_T interval to get an estimate of the Λ_c^+ cross section value in $0 < p_T < 1$ GeV/c, and then integrating in p_T. The results obtained with the two methods were found to be compatible within the uncertainties.

The resulting p_T-integrated cross section of the Λ_c^+ baryon in pp collisions at $\sqrt{s} = 5.02$ TeV is

$$\mathrm{d}\sigma^{\Lambda_c^+}_{\mathrm{pp,\ 5.02\ TeV}}/\mathrm{d}y|_{|y|<0.5} = 278 \pm 16\ (\mathrm{stat.}) \pm 24\ (\mathrm{syst.}) \pm 7\ (\mathrm{lumi.})^{+6}_{-12}\ (\mathrm{extrap.})\ \mu\mathrm{b}. \tag{9}$$

In p–Pb collisions, the p_T-integrated Λ_c^+-production cross section was obtained using a different approach, since the p_T spectrum of Λ_c^+ is not well described by PYTHIA or other event generators. In this case, the cross sections in $0 < p_T < 1$ GeV/c and $p_T > 24$ GeV/c were calculated as the product of the pp cross sections in these p_T intervals obtained from the extrapolation of the measured p_T-differential cross section, as described above; the Pb mass number; a correction factor to account for the different rapidity interval covered in pp and p–Pb collisions; and an assumption on the nuclear modification factor R_{pPb} as described hereafter. For $0 < p_T < 1$ GeV/c, the R_{pPb} was taken as $R_{pPb} = 0.5$ as in the $1 < p_T < 2$ GeV/c interval, under the hypothesis that the trend of the Λ_c^+ R_{pPb} at low p_T is similar to that of D mesons. The uncertainty was estimated by varying the hypothesis in the range $0.35 < R_{pPb} < 0.8$, which incorporates the envelope of the available models (see Fig. 8) and the range defined by the combination of the statistical and systematic uncertainties of the Λ_c^+ R_{pPb} in $1 < p_T < 2$ GeV/c. For $p_T > 24$ GeV/c, the R_{pPb} was assumed to be equal to unity, with the range $0.8 < R_{pPb} < 1.2$ used to define the uncertainty.

The resulting p_T-integrated cross section of prompt Λ_c^+ in p–Pb collisions at $\sqrt{s_{NN}} = 5.02$ TeV is

$$d\sigma^{\Lambda_c^+}_{\mathrm{pPb,\ 5.02\ TeV}}/dy|_{-0.96<y<0.04} = 39.6 \pm 2.7\ (\mathrm{stat.}) \pm 4.2\ (\mathrm{syst.}) \pm 1.5\ (\mathrm{lumi.})^{+5.3}_{-3.5}\ (\mathrm{extrap.})\,\mathrm{mb}. \quad (10)$$

The visible cross sections make up 70% and 80% of the integrated cross sections in pp and p–Pb collisions, respectively. The p_T-integrated Λ_c^+ cross sections in pp and p–Pb collisions can be used for the comparison of fragmentation fractions of charm quarks in different collision systems and rapidity intervals. They can also be used in the calculation of the $c\bar{c}$ cross section together with the cross sections of D mesons and higher-mass charmed baryons that do not decay into Λ_c^+. Due to the lack of measurements of higher-mass charmed baryons ($\Xi_c^{+,0}, \Omega_c$) at $\sqrt{s} = 5.02$ TeV, which contribute to the $c\bar{c}$ cross section, a calculation of the $c\bar{c}$ cross section is beyond the scope of this work.

6.4 Λ_c^+/D^0 ratios

The ratios between the yields of Λ_c^+ baryons and D^0 mesons were calculated using the D^0 cross sections reported in [89] for pp collisions and [90] for p–Pb collisions, respectively. The uncertainty sources assumed to be uncorrelated between the Λ_c^+ and D^0 production cross sections include those due to the raw-yield extraction, the selection efficiency, the PID efficiency, the generated p_T shape, the $(A \times \varepsilon)$ statistical uncertainties, and the branching ratios. The uncertainties assumed to be correlated include those due to the tracking, the beauty feed-down and the luminosity. The D^0 cross section was measured in finer p_T intervals than the Λ_c^+, so it was rebinned such that the p_T intervals match between the two species.

The Λ_c^+/D^0 ratio as a function of p_T in pp and p–Pb collisions is shown in Fig. 9. A clear decreasing trend with increasing p_T is seen in both pp and p–Pb collisions for $p_T > 2$ GeV/c, and at high p_T the ratio reaches a value of about 0.2. The ratios measured in pp and p–Pb collisions are qualitatively consistent with each other, although there is a hint of a larger Λ_c^+/D^0 ratio in $5 < p_T < 8$ GeV/c and a lower ratio in $1 < p_T < 2$ GeV/c in p–Pb collisions with respect to pp collisions.

The values of the p_T-integrated Λ_c^+/D^0 ratios are reported in Tab. 3 along with the values measured in e^+e^- and e^-p collisions by other experiments. The Λ_c^+/D^0 ratios in pp and p–Pb collisions are consistent with each other within 2σ. Comparing to previous measurements in other collision systems, the Λ_c^+/D^0 ratio is significantly enhanced by a factor of about 3–5 in pp collisions and a factor of about 2–4 in p–Pb collisions, indicating that the fragmentation fractions of charm quarks into baryons are different with respect to e^+e^- and e^-p collisions. This is consistent with the previous ALICE measurements [5], where the p_T-integrated Λ_c^+/D^0 ratios were restricted to $1 < p_T < 8$ GeV/c in pp collisions, and to $2 < p_T < 12$ GeV/c in p–Pb collisions.

Figure 10 shows the Λ_c^+/D^0 ratio in pp collisions compared with models from MC generators, and a statistical hadronisation model. The MC generators include PYTHIA 8 with Monash tune and colour reconnection tunes as described above; PYTHIA 8 with colour reconnection plus rope hadronisation [14, 91] where colour charges can act coherently to form a rope, increasing the effective string tension; HERWIG 7 [17] where hadronisation is implemented via clusters; and POWHEG pQCD generator matched to PYTHIA 6 to generate the parton shower, as described above. The measured points are also compared to predictions from GM-VFNS pQCD calculations, which were computed as the ratios of the Λ_c^+ and D^0 cross sections obtained with the same choice of pQCD scales [86]. The left panel shows the predictions of the Λ_c^+/D^0 ratio from PYTHIA 8 (Monash tune), HERWIG 7, POWHEG, and GM-VFNS, which all implement fragmentation processes tuned on charm production measurements in e^+e^- collisions, and

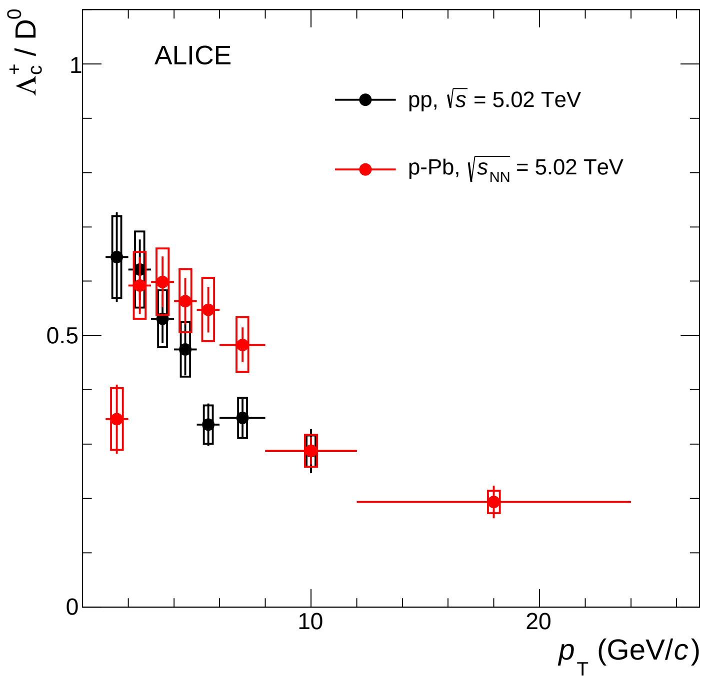

Figure 9: The Λ_c^+/D^0 ratio as a function of p_T measured in pp collisions at $\sqrt{s} = 5.02$ TeV and in p–Pb collisions at $\sqrt{s_{NN}} = 5.02$ TeV.

	$\Lambda_c^+/D^0 \pm$ stat. $\pm$ syst.	System	$\sqrt{s}$ (GeV)	Notes
ALICE	$0.62 \pm 0.05 \pm 0.05\,^{+0.01}_{-0.03}$	pp	5020	$p_T > 0, \lvert y\rvert < 0.5$
ALICE	$0.45 \pm 0.03 \pm 0.06^{+0.06}_{-0.04}$	p–Pb	5020	$p_T > 0, -0.96 < y < 0.04$
CLEO [7]	$0.119 \pm 0.021 \pm 0.019$	e^+e^-	10.55	
ARGUS [6, 8]	0.127 ± 0.031	e^+e^-	10.55	
LEP average [9]	$0.113 \pm 0.013 \pm 0.006$	e^+e^-	91.2	
ZEUS DIS [12]	$0.124 \pm 0.034^{+0.025}_{-0.022}$	e^-p	320	$1 < Q^2 < 1000$ GeV^2, $0 < p_T < 10$ GeV/c, $0.02 < y < 0.7$
ZEUS γp, HERA I [10]	$0.220 \pm 0.035^{+0.027}_{-0.037}$	e^-p	320	$130 < W < 300$ GeV, $Q^2 < 1$ GeV^2, $p_T > 3.8$ GeV/c, $\lvert\eta\rvert < 1.6$
ZEUS γp, HERA II [11]	$0.107 \pm 0.018^{+0.009}_{-0.014}$	e^-p	320	$130 < W < 300$ GeV, $Q^2 < 1$ GeV^2, $p_T > 3.8$ GeV/c, $\lvert\eta\rvert < 1.6$

Table 3: Comparison of the p_T-integrated Λ_c^+/D^0 ratio measured in pp and p–Pb collisions, and the same ratios in e^+e^- and e^-p collisions (reproduced from [5]). Statistical and systematic uncertainties are reported (from references [6, 8] it was not possible to separate systematics and statistical uncertainties). The ALICE measurements report an additional uncertainty source from the extrapolation procedure.

therefore all predict a value of the Λ_c^+/D^0 ratio around 0.1, with a very mild p_T dependence. These predictions significantly underestimate the data at low p_T by a factor of about 6–10, while at high p_T the discrepancy is reduced to a factor of about 3. The right panel shows models which include processes that enhance baryon production. A significant enhancement of the Λ_c^+/D^0 ratio is observed with PYTHIA

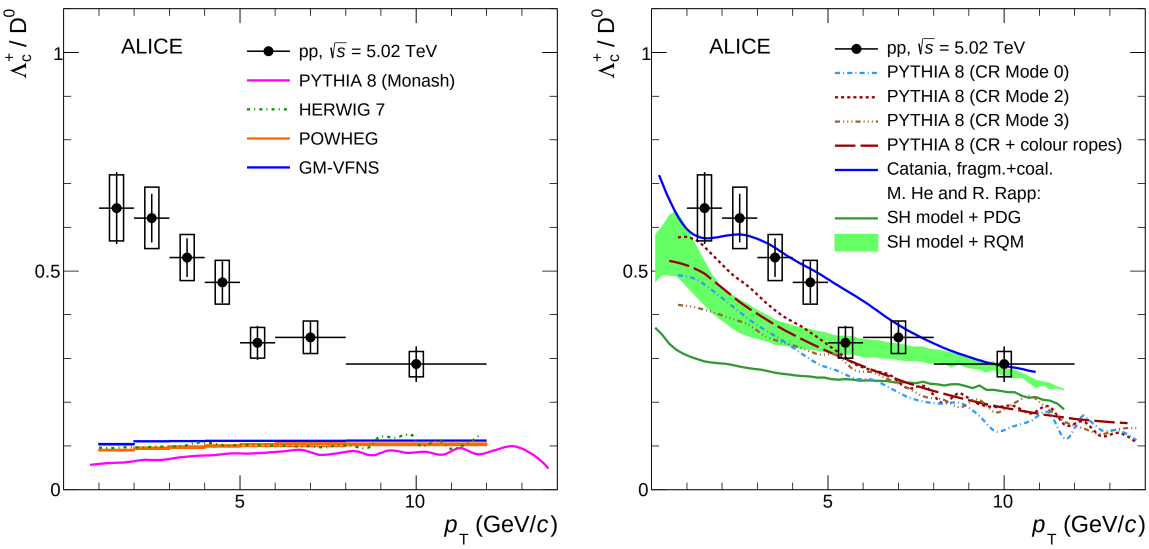

Figure 10: The Λ_c^+/D^0 ratio measured in pp collisions at $\sqrt{s} = 5.02$ TeV, compared to theoretical predictions. The measurement is compared with predictions from MC generators (PYTHIA 8 [13, 14], HERWIG 7 [17], POWHEG [84]), GM-VFNS [86], a statistical hadronisation model [60] ('SH model' in the legend) and a model which implements hadronisation via coalescence and fragmentation [93]. See text for model details.

8 simulations including CR beyond the leading-colour approximation, with respect to the Monash tune. The results of these PYTHIA 8 tunes are qualitatively consistent with the measured Λ_c^+/D^0 ratio in pp collisions at both energies, also reproducing the decreasing trend of Λ_c^+/D^0 with increasing p_T. Including rope hadronisation in addition to colour reconnection induces a small modification in the Λ_c^+/D^0 ratio, suggesting that the increased string tension does not significantly affect the relative production of baryons with respect to mesons. The data is also compared with a statistical hadronisation model [60] where the underlying charmed baryon spectrum is either taken from the PDG, or augmented to include additional excited baryon states, which have not yet been observed but are predicted by the Relativistic Quark Model (RQM) [92]. For the former case, the model underpredicts the data, especially at low p_T. For the latter case, the additional charmed baryon states decay strongly to Λ_c^+ baryons, contributing to the prompt Λ_c^+ spectrum. This increases the Λ_c^+/D^0 ratio and allows the model to get closer to the data, and also describe the p_T dependence of the measured ratio. Finally, the Catania model [93] is also presented, which assumes that a QGP is formed in pp collisions and that the hadronisation occurs via coalescence as well as fragmentation. The light quark p_T spectrum is determined with a blast wave model, while the heavy quark p_T spectrum is determined with FONLL pQCD predictions, and coalescence is implemented via the Wigner formalism. Contrary to the implementation in Pb–Pb collisions [93], jet quenching mechanisms are not included in pp collisions. The model predicts that hadronisation via coalescence is dominant at low p_T, while fragmentation dominates at high p_T. Both the magnitude and the p_T shape of the measured Λ_c^+/D^0 ratio are described well by this model.

Figure 11 (left) shows the Λ_c^+/D^0 ratio in pp collisions at $\sqrt{s} = 5.02$ TeV compared with the previous measurement at $\sqrt{s} = 7$ TeV, and with predictions from PYTHIA 8 simulations. The Λ_c^+/D^0 ratio is found to be consistent between the two collision energies, within the experimental uncertainties; however, the wider p_T coverage and the improved statistical and systematic uncertainties on the new measurement reveal a clear decreasing trend in the Λ_c^+/D^0 ratio in pp collisions at $\sqrt{s} = 5.02$ TeV, which was not clearly visible in the result at $\sqrt{s} = 7$ TeV. The predictions of PYTHIA 8 with Monash tune do not show a $\sqrt{s}$-dependence, while those with CR Mode 2 indicate a slight $\sqrt{s}$-dependence, where the Λ_c^+/D^0 ratio is slightly larger at low p_T at $\sqrt{s} = 7$ TeV than at $\sqrt{s} = 5.02$ TeV. The right panel shows the Λ_c^+/D^0 ratio in pp collisions, compared with the measurement by the CMS Collaboration in $5 < p_T < 20$ GeV/c and

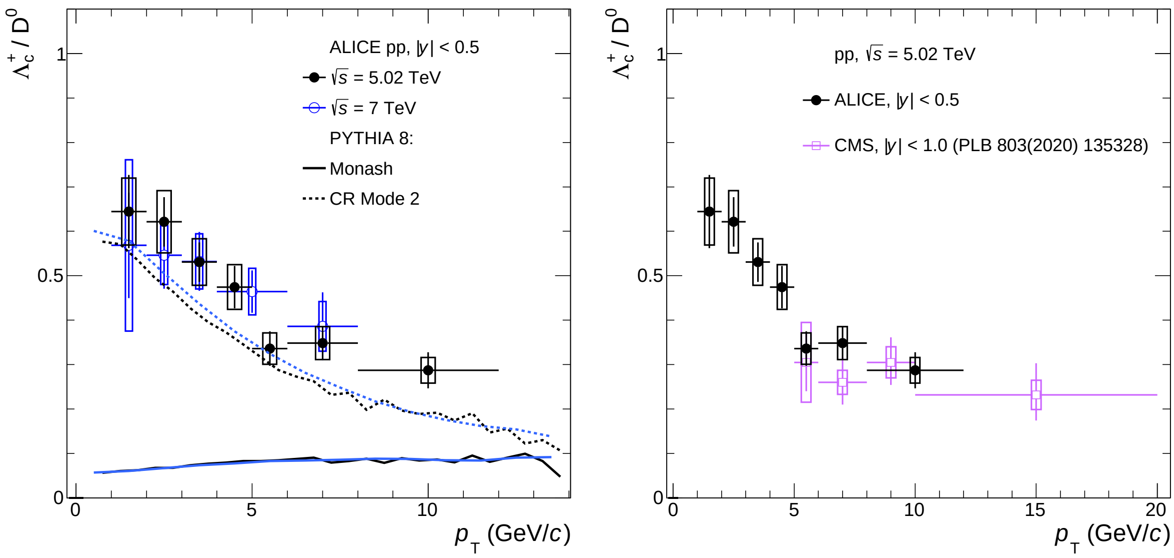

Figure 11: Left: The Λ_c^+/D^0 ratio measured in pp collisions at $\sqrt{s} = 5.02$ TeV, compared to the measurement at $\sqrt{s} = 7$ TeV [5]. PYTHIA 8 predictions are shown at both energies, for the Monash tune (solid lines) and with the Mode 2 CR tune (dotted lines). Right: the Λ_c^+/D^0 ratio at $\sqrt{s} = 5.02$ TeV compared with the measurement by the CMS Collaboration at $|y| < 1$ [18].

$|y| < 1$ [18]. In the p_T region covered by both experiments, the results are found to be consistent with one another.

In Fig. 12, the Λ_c^+/D^0 ratio in p–Pb collisions at midrapidity ($-0.96 < y < 0.04$) is compared with the measurements by the LHCb Collaboration at forward ($1.5 < y < 4$) and backward ($-4.5 < y < -2.5$) rapidities [59]. The left panel shows the comparison of the Λ_c^+/D^0 ratios in the different rapidity intervals as a function of p_T. For $p_T < 8$ GeV$/c$ the ratio measured at midrapidity is higher than the ones measured at forward and backward rapidities, whereas at higher p_T the measurements are consistent within uncertainties. The right panel shows the p_T-integrated Λ_c^+/D^0 ratio as a function of rapidity. The p_T range of the integration of the ALICE data ($2 < p_T < 12$ GeV$/c$) is chosen to be similar to the reported LHCb integrated p_T range ($2 < p_T < 10$ GeV$/c$). The results suggest an enhancement of the ratio at midrapidity with respect to forward and backward rapidities. The difference between the Λ_c^+/D^0 ratio at mid and forward (backward) rapidities is less pronounced in p–Pb collisions compared to the one observed in pp collisions at 7 TeV [5, 19].

Figure 13 shows the Λ_c^+/D^0 ratio in pp and p–Pb collisions, compared to the baryon-to-meson ratios in the light flavour sector, p/π [55, 94] and Λ/K_S^0 [95, 96]. The p/π ratio in pp collisions is shown at centre-of-mass energies of 7 TeV and 5.02 TeV, and both results are fully consistent with each other. The Λ/K_S^0 ratio in pp collisions is shown at $\sqrt{s} = 7$ TeV. Comparing the Λ_c^+/D^0 ratio to the light-flavour ratios, similar characteristics can be seen. All the baryon-to-meson ratios decrease with increasing p_T for $p_T > 3$ GeV$/c$. In addition, the light-flavour hadron ratios show a distinct peak at intermediate p_T (around 3 GeV$/c$), while the Λ_c^+/D^0 ratio shows a hint of a peak at $2 < p_T < 4$ GeV$/c$ in p–Pb collisions, though a higher precision measurement would be needed to confirm this. Also shown in Fig. 13 are predictions from PYTHIA 8 with Monash and CR Mode 2 tunes. The PYTHIA 8 predictions for the light-flavour baryon-to-meson ratios are calculated at $\sqrt{s} = 7$ TeV. It can be observed that the behaviours of the PYTHIA 8 predictions for light-flavour and charm baryon-to-meson ratios are similar. The measured Λ/K_S^0 ratio in pp collisions is underestimated by the Monash tune, while for the CR Mode 2 tune both the magnitude and trend of the ratio are closer to data, despite predicting a slightly flatter trend with p_T. The p/π ratio ratio is underestimated by PYTHIA 8 (Monash) at low p_T but overestimated at high p_T, while CR Mode 2 improves the agreement with data at low p_T but still overestimates the data at high p_T.

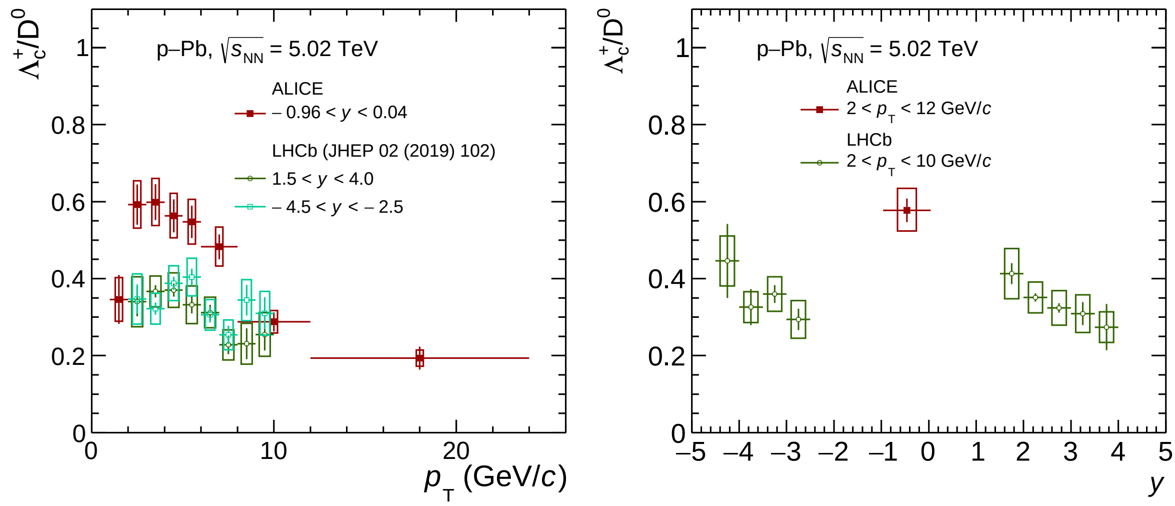

Figure 12: The Λ_c^+/D^0 ratio measured in p–Pb collisions at $\sqrt{s_{NN}} = 5.02$ TeV, compared with the measurement at forward and backward rapidity [59] by the LHCb collaboration. The measurements are shown as a function of p_T (left) and as a function of y (right).

Overall, the colour reconnection modes in PYTHIA 8 generally provide for a better description of the baryon-to-meson ratios in both the light-flavour and charm sector.

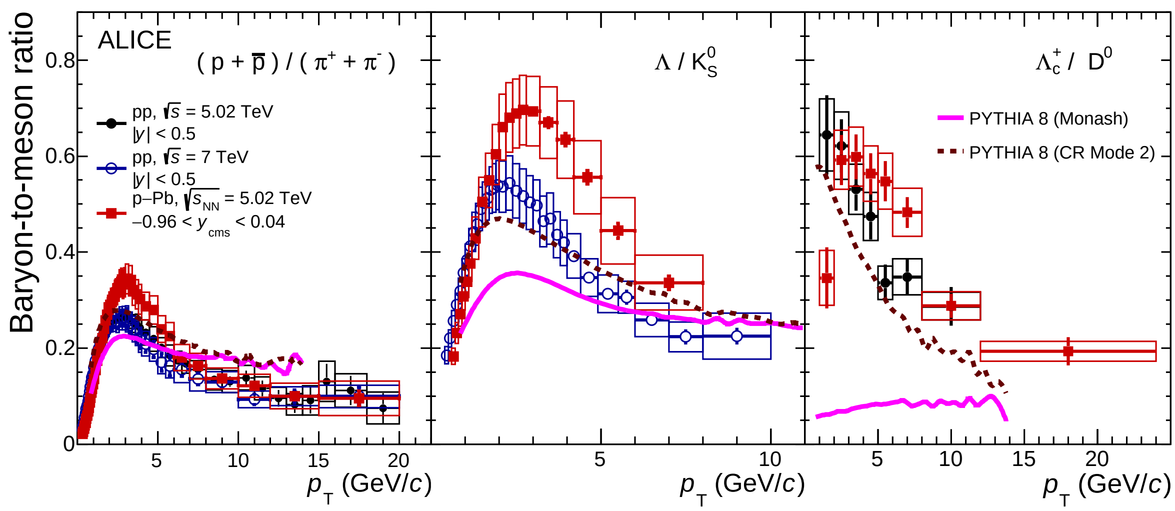

Figure 13: The baryon-to-meson ratios in the light-flavour and charm sector; p/π in pp collisions at $\sqrt{s} = 5.02$ TeV and 7 TeV and p–Pb collisions at $\sqrt{s_{NN}} = 5.02$ TeV [55] (left), Λ/K^0_S in pp collisions at $\sqrt{s} = 7$ TeV and p–Pb collisions at $\sqrt{s_{NN}} = 5.02$ TeV [95, 96] (middle), and Λ_c^+/D^0 in pp collisions at $\sqrt{s} = 5.02$ TeV and p–Pb collisions at $\sqrt{s_{NN}} = 5.02$ TeV (right). The data are compared to predictions from PYTHIA 8 [13, 14]. See text for model details.

7 Summary and conclusions

The measurements of the production of prompt Λ_c^+ baryons at midrapidity in pp collisions at $\sqrt{s} = 5.02$ TeV and in p–Pb collisions at $\sqrt{s_{NN}} = 5.02$ TeV with the ALICE detector at the LHC have been reported. The measurement in pp collisions, in particular, was performed at a different centre-of-mass energy with respect to the previous work in which Λ_c^+-baryon production was measured in pp collisions at $\sqrt{s} = 7$ TeV [5]. The pp data sample at $\sqrt{s} = 5.02$ TeV is the natural reference for measurements in p–Pb and Pb–Pb collisions at the same centre-of-mass energy per nucleon pair. Moreover, with respect to [5], the uncertainties were significantly reduced, and the p_T range and the p_T granularity of the measurements were improved in both collision systems. The analysis was performed using two different decay channels, $\Lambda_c^+ \to pK^-\pi^+$ and $\Lambda_c^+ \to pK_S^0$, and two different analysis methods, a procedure based on rectangular selections and a multivariate analysis technique. The results were reported for pp collisions in the rapidity interval $|y| < 0.5$ and the transverse-momentum interval $1 < p_T < 12$ GeV/c and for p–Pb collisions in $-0.96 < y < 0.04$ and $1 < p_T < 24$ GeV/c. The p_T-differential production cross sections were obtained averaging the results from different hadronic decay channels and different analysis approaches.

The p_T-differential cross section was measured to be larger than predictions given by pQCD calculations in both pp and p–Pb collisions. The nuclear modification factor R_{pPb} of Λ_c^+ baryons was found to be below unity in the interval $1 < p_T < 2$ GeV/c and above unity at mid-p_T although compatible with unity within uncertainties. It is also consistent with the R_{pPb} of D mesons within uncertainties. The current precision of the measurement is not enough to draw conclusions on the role of different CNM effects and the possible presence of hot-medium effects. As already observed in [5], the Λ_c^+/D^0 baryon-to-meson ratio in pp collisions is larger than previous measurements obtained in e^+e^- and e^-p collision systems at lower centre-of-mass energies. The increase of precision in this paper allowed to observe, for the first time, a clear decreasing trend as a function of transverse momentum in the Λ_c^+/D^0 ratio. The Λ_c^+/D^0 ratio was compared to pp event generators and models that implement different particle production and hadronisation mechanisms: qualitative agreement with the measurement is obtained with PYTHIA 8 tunes including string formation beyond the leading-colour approximation; a prediction based on the statistical hadronisation model which includes unobserved charmed baryon states that strongly decay to Λ_c^+; and a prediction which assumes the formation of a QGP and implements hadronisation via coalescence and fragmentation. The Λ_c^+/D^0 ratio measured in pp collisions is consistent with the results by CMS at midrapidity in the common p_T regions of both measurements. The ratio in p–Pb collisions at midrapidity is higher than the one measured by LHCb at forward and backward rapidities in $2 < p_T < 8$ GeV/c, while for $p_T > 8$ GeV/c the measurements at central, forward and backward rapidities are consistent within uncertainties. The measured Λ_c^+/D^0 ratio was also compared with baryon-to-meson ratios measured in the light-flavour sector. The measured Λ/K_S^0 ratio can also be described by PYTHIA 8 when including string formation beyond the leading-colour approximation, although this PYTHIA 8 tune slightly overestimates the measured p/π ratio. The increased precision of this measurement with respect to the measurements made with the Run 1 data is crucial for providing further insight into charmed baryon production in pp and p–Pb collisions. A more precise measurement is expected to be obtained during the LHC Run 3 and Run 4 after the upgrade of the ALICE apparatus [97].

Acknowledgements

The ALICE Collaboration would like to thank all its engineers and technicians for their invaluable contributions to the construction of the experiment and the CERN accelerator teams for the outstanding performance of the LHC complex. The ALICE Collaboration gratefully acknowledges the resources and support provided by all Grid centres and the Worldwide LHC Computing Grid (WLCG) collaboration. The ALICE Collaboration acknowledges the following funding agencies for their support in building and running the ALICE detector: A. I. Alikhanyan National Science Laboratory (Yerevan Physics Institute) Foundation (ANSL), State Committee of Science and World Federation of Scientists (WFS), Armenia; Austrian Academy of Sciences, Austrian Science Fund (FWF): [M 2467-N36] and Nationalstiftung für Forschung, Technologie und Entwicklung, Austria; Ministry of Communications and High Technologies, National Nuclear Research Center, Azerbaijan; Conselho Nacional de Desenvolvimento Científico e Tecnológico (CNPq), Financiadora de Estudos e Projetos (Finep), Fundação de Amparo à Pesquisa do Estado de São Paulo (FAPESP) and Universidade Federal do Rio Grande do Sul (UFRGS), Brazil; Ministry of Education of China (MOEC) , Ministry of Science & Technology of China (MSTC) and National Natural Science Foundation of China (NSFC), China; Ministry of Science and Education and Croatian Science Foundation, Croatia; Centro de Aplicaciones Tecnológicas y Desarrollo Nuclear (CEADEN), Cubaenergía, Cuba; Ministry of Education, Youth and Sports of the Czech Republic, Czech Republic; The Danish Council for Independent Research | Natural Sciences, the VILLUM FONDEN and Danish National Research Foundation (DNRF), Denmark; Helsinki Institute of Physics (HIP), Finland; Commissariat à l'Energie Atomique (CEA) and Institut National de Physique Nucléaire et de Physique des Particules (IN2P3) and Centre National de la Recherche Scientifique (CNRS), France; Bundesministerium für Bildung und Forschung (BMBF) and GSI Helmholtzzentrum für Schwerionenforschung GmbH, Germany; General Secretariat for Research and Technology, Ministry of Education, Research and Religions, Greece; National Research, Development and Innovation Office, Hungary; Department of Atomic Energy Government of India (DAE), Department of Science and Technology, Government of India (DST), University Grants Commission, Government of India (UGC) and Council of Scientific and Industrial Research (CSIR), India; Indonesian Institute of Science, Indonesia; Istituto Nazionale di Fisica Nucleare (INFN), Italy; Institute for Innovative Science and Technology , Nagasaki Institute of Applied Science (IIST), Japanese Ministry of Education, Culture, Sports, Science and Technology (MEXT) and Japan Society for the Promotion of Science (JSPS) KAKENHI, Japan; Consejo Nacional de Ciencia (CONACYT) y Tecnología, through Fondo de Cooperación Internacional en Ciencia y Tecnología (FONCICYT) and Dirección General de Asuntos del Personal Academico (DGAPA), Mexico; Nederlandse Organisatie voor Wetenschappelijk Onderzoek (NWO), Netherlands; The Research Council of Norway, Norway; Commission on Science and Technology for Sustainable Development in the South (COMSATS), Pakistan; Pontificia Universidad Católica del Perú, Peru; Ministry of Science and Higher Education, National Science Centre and WUT ID-UB, Poland; Korea Institute of Science and Technology Information and National Research Foundation of Korea (NRF), Republic of Korea; Ministry of Education and Scientific Research, Institute of Atomic Physics and Ministry of Research and Innovation and Institute of Atomic Physics, Romania; Joint Institute for Nuclear Research (JINR), Ministry of Education and Science of the Russian Federation, National Research Centre Kurchatov Institute, Russian Science Foundation and Russian Foundation for Basic Research, Russia; Ministry of Education, Science, Research and Sport of the Slovak Republic, Slovakia; National Research Foundation of South Africa, South Africa; Swedish Research Council (VR) and Knut & Alice Wallenberg Foundation (KAW), Sweden; European Organization for Nuclear Research, Switzerland; Suranaree University of Technology (SUT), National Science and Technology Development Agency (NSDTA) and Office of the Higher Education Commission under NRU project of Thailand, Thailand; Turkish Atomic Energy Agency (TAEK), Turkey; National Academy of Sciences of Ukraine, Ukraine; Science and Technology Facilities Council (STFC), United Kingdom; National Science Foundation of the United States of America (NSF) and United States Department of Energy, Office of Nuclear Physics (DOE NP), United States of America.

References

[1] B. A. Kniehl, G. Kramer, I. Schienbein, and H. Spiesberger, "Collinear subtractions in hadroproduction of heavy quarks", *Eur. Phys. J.* **C41** (2005) 199–212, `arXiv:hep-ph/0502194 [hep-ph]`.

[2] B. A. Kniehl, G. Kramer, I. Schienbein, and H. Spiesberger, "Inclusive Charmed-Meson Production at the CERN LHC", *Eur. Phys. J.* **C72** (2012) 2082, `arXiv:1202.0439 [hep-ph]`.

[3] M. Cacciari, M. Greco, and P. Nason, "The p_T Spectrum in Heavy-Flavour Hadroproduction", *JHEP* **05** (1998) 007, `arXiv:hep-ph/9803400 [hep-ph]`.

[4] M. Cacciari *et al.*, "Theoretical predictions for charm and bottom production at the LHC", *JHEP* **10** (2012) 137, `arXiv:1205.6344 [hep-ph]`.

[5] **ALICE** Collaboration, S. Acharya *et al.*, "Λ_c^+ production in pp collisions at $\sqrt{s} = 7$ TeV and in p-Pb collisions at $\sqrt{s_{NN}} = 5.02$ TeV", *JHEP* **04** (2018) 108, `arXiv:1712.09581 [nucl-ex]`.

[6] **ARGUS** Collaboration, H. Albrecht *et al.*, "Observation of the charmed baryon Λ_c in e^+e^- annihilation at 10-GeV", *Phys. Lett.* **B207** (1988) 109–114.

[7] **CLEO** Collaboration, P. Avery *et al.*, "Inclusive production of the charmed baryon Λ_c from e^+e^- annihilations at $\sqrt{s} = 10.55$ GeV", *Phys. Rev.* **D43** (1991) 3599–3610.

[8] **ARGUS** Collaboration, H. Albrecht *et al.*, "Inclusive production of D^0, D^+ and $D^*(2010)^+$ mesons in B decays and nonresonant e^+e^- annihilation at 10.6 GeV", *Z. Phys.* **C52** (1991) 353–360.

[9] L. Gladilin, "Fragmentation fractions of c and b quarks into charmed hadrons at LEP", *Eur. Phys. J.* **C75** no. 1, (2015) 19, `arXiv:1404.3888 [hep-ex]`.

[10] **ZEUS** Collaboration, S. Chekanov *et al.*, "Measurement of charm fragmentation ratios and fractions in photoproduction at HERA", *Eur. Phys. J.* **C44** (2005) 351–366, `arXiv:hep-ex/0508019 [hep-ex]`.

[11] **ZEUS** Collaboration, H. Abramowicz *et al.*, "Measurement of charm fragmentation fractions in photoproduction at HERA", *JHEP* **09** (2013) 058, `arXiv:1306.4862 [hep-ex]`.

[12] **ZEUS** Collaboration, H. Abramowicz *et al.*, "Measurement of D^+ and Λ_c^+ production in deep inelastic scattering at HERA", *JHEP* **11** (2010) 009, `arXiv:1007.1945 [hep-ex]`.

[13] P. Skands, S. Carrazza, and J. Rojo, "Tuning PYTHIA 8.1: the Monash 2013 Tune", *Eur. Phys. J.* **C74** no. 8, (2014) 3024, `arXiv:1404.5630 [hep-ph]`.

[14] J. R. Christiansen and P. Z. Skands, "String Formation Beyond Leading Colour", *JHEP* **08** (2015) 003, `arXiv:1505.01681 [hep-ph]`.

[15] C. Bierlich and J. R. Christiansen, "Effects of color reconnection on hadron flavor observables", *Phys. Rev.* **D92** no. 9, (2015) 094010, `arXiv:1507.02091 [hep-ph]`.

[16] C. Flensburg, G. Gustafson, and L. Lonnblad, "Inclusive and Exclusive Observables from Dipoles in High Energy Collisions", *JHEP* **08** (2011) 103, `arXiv:1103.4321 [hep-ph]`.

[17] M. Bahr *et al.*, "Herwig++ Physics and Manual", *Eur. Phys. J.* **C58** (2008) 639–707, `arXiv:0803.0883 [hep-ph]`.

[18] **CMS** Collaboration, A. M. Sirunyan *et al.*, "Production of Λ_c^+ baryons in proton-proton and lead-lead collisions at $\sqrt{s_{NN}} = 5.02$ TeV", *Phys. Lett. B* **803** (2020) 135328, `arXiv:1906.03322 [hep-ex]`.

[19] **LHCb** Collaboration, R. Aaij *et al.*, "Prompt charm production in pp collisions at $\sqrt{s} = 7$ TeV", *Nucl. Phys.* **B871** (2013) 1–20, `arXiv:1302.2864 [hep-ex]`.

[20] R. Maciula and A. Szczurek, "Production of Λ_c baryons at the LHC within the k_T-factorization approach and independent parton fragmentation picture", *Phys. Rev.* **D98** no. 1, (2018) 014016, `arXiv:1803.05807 [hep-ph]`.

[21] **LHCb** Collaboration, R. Aaij *et al.*, "Measurement of b-hadron production fractions in 7 TeV pp collisions", *Phys. Rev.* **D85** (2012) 032008, `arXiv:1111.2357 [hep-ex]`.

[22] **LHCb** Collaboration, R. Aaij *et al.*, "Study of the production of Λ_b^0 and $\overline{B}^0$ hadrons in pp collisions and first measurement of the $\Lambda_b^0 \to J/\psi pK^-$ branching fraction", *Chin. Phys. C* **40** no. 1, (2016) 011001, `arXiv:1509.00292 [hep-ex]`.

[23] **LHCb** Collaboration, R. Aaij *et al.*, "Measurement of b hadron fractions in 13 TeV pp collisions", *Phys. Rev.* **D100** no. 3, (2019) 031102, `arXiv:1902.06794 [hep-ex]`.

[24] **CMS** Collaboration, S. Chatrchyan *et al.*, "Measurement of the Λ_b cross section and the $\overline{\Lambda}_b$ to Λ_b ratio with $J/\Psi\Lambda$ decays in pp collisions at $\sqrt{s} = 7$ TeV", *Phys. Lett.* **B714** (2012) 136–157, `arXiv:1205.0594 [hep-ex]`.

[25] **STAR** Collaboration, J. Adams *et al.*, "Experimental and theoretical challenges in the search for the quark gluon plasma: The STAR Collaboration's critical assessment of the evidence from RHIC collisions", *Nucl. Phys.* **A757** (2005) 102–183, `arXiv:nucl-ex/0501009 [nucl-ex]`.

[26] **PHENIX** Collaboration, K. Adcox *et al.*, "Formation of dense partonic matter in relativistic nucleus-nucleus collisions at RHIC: Experimental evaluation by the PHENIX collaboration", *Nucl. Phys.* **A757** (2005) 184–283, `arXiv:nucl-ex/0410003 [nucl-ex]`.

[27] **BRAHMS** Collaboration, I. Arsene *et al.*, "Quark gluon plasma and color glass condensate at RHIC? The Perspective from the BRAHMS experiment", *Nucl. Phys.* **A757** (2005) 1–27, `arXiv:nucl-ex/0410020 [nucl-ex]`.

[28] V. Greco, C. M. Ko, and R. Rapp, "Quark coalescence for charmed mesons in ultrarelativistic heavy ion collisions", *Phys. Lett.* **B595** (2004) 202–208, `arXiv:nucl-th/0312100 [nucl-th]`.

[29] Y. Oh, C. M. Ko, S. H. Lee, and S. Yasui, "Heavy baryon/meson ratios in relativistic heavy ion collisions", *Phys. Rev.* **C79** (2009) 044905, `arXiv:0901.1382 [nucl-th]`.

[30] **STAR** Collaboration, J. Adam *et al.*, "Observation of enhancement of charmed baryon-to-meson ratio in Au+Au collisions at $\sqrt{s_{NN}}$ = 200 GeV", *Phys. Rev. Lett.* **124** no. 17, (2020) 172301, `arXiv:1910.14628 [nucl-ex]`.

[31] **ALICE** Collaboration, S. Acharya *et al.*, "Λ_c^+ production in Pb-Pb collisions at $\sqrt{s_{\rm NN}} = 5.02$ TeV", *Phys. Lett.* **B793** (2019) 212–223, `arXiv:1809.10922 [nucl-ex]`.

[32] S. H. Lee, K. Ohnishi, S. Yasui, I.-K. Yoo, and C.-M. Ko, "Λ_c enhancement from strongly coupled quark-gluon plasma", *Phys. Rev. Lett.* **100** (2008) 222301, `arXiv:0709.3637 [nucl-th]`.

[33] J. Zhao, S. Shi, N. Xu, and P. Zhuang, "Sequential Coalescence with Charm Conservation in High Energy Nuclear Collisions", `arXiv:1805.10858 [hep-ph]`.

[34] S. Cho, K.-J. Sun, C. M. Ko, S. H. Lee, and Y. Oh, "Charmed hadron production in an improved quark coalescence model", *Phys. Rev. C* **101** no. 2, (2020) 024909, `arXiv:1905.09774 [nucl-th]`.

[35] M. He and R. Rapp, "Hadronization and Charm-Hadron Ratios in Heavy-Ion Collisions", *Phys. Rev. Lett.* **124** no. 4, (2020) 042301, `arXiv:1905.09216 [nucl-th]`.

[36] M. Arneodo, "Nuclear effects in structure functions", *Physics Reports* **240** no. 5, (1994) 301 – 393.

[37] S. Malace, D. Gaskell, D. W. Higinbotham, and I. Cloet, "The Challenge of the EMC Effect: existing data and future directions", *Int. J. Mod. Phys.* **E23** no. 08, (2014) 1430013, `arXiv:1405.1270 [nucl-ex]`.

[38] K. J. Eskola, P. Paakkinen, H. Paukkunen, and C. A. Salgado, "EPPS16: Nuclear parton distributions with LHC data", *Eur. Phys. J.* **C77** no. 3, (2017) 163, arXiv:1612.05741 [hep-ph].

[39] K. Kovarik *et al.*, "nCTEQ15 - Global analysis of nuclear parton distributions with uncertainties in the CTEQ framework", *Phys. Rev. D* **93** no. 8, (2016) 085037, arXiv:1509.00792 [hep-ph].

[40] F. Gelis, E. Iancu, J. Jalilian-Marian, and R. Venugopalan, "The Color Glass Condensate", *Ann. Rev. Nucl. Part. Sci.* **60** (2010) 463–489, arXiv:1002.0333 [hep-ph].

[41] P. Tribedy and R. Venugopalan, "QCD saturation at the LHC: Comparisons of models to p + p and A + A data and predictions for p + Pb collisions", *Phys. Lett.* **B710** (2012) 125–133, arXiv:1112.2445 [hep-ph]. [Erratum: Phys. Lett.B718,1154(2013)].

[42] J. L. Albacete, A. Dumitru, H. Fujii, and Y. Nara, "CGC predictions for p + Pb collisions at the LHC", *Nucl. Phys.* **A897** (2013) 1–27, arXiv:1209.2001 [hep-ph].

[43] A. H. Rezaeian, "CGC predictions for p+A collisions at the LHC and signature of QCD saturation", *Phys. Lett.* **B718** (2013) 1058–1069, arXiv:1210.2385 [hep-ph].

[44] H. Fujii and K. Watanabe, "Heavy quark pair production in high energy pA collisions: Open heavy flavors", *Nucl. Phys.* **A920** (2013) 78–93, arXiv:1308.1258 [hep-ph].

[45] I. Vitev, "Non-Abelian energy loss in cold nuclear matter", *Phys. Rev.* **C75** (2007) 064906, arXiv:hep-ph/0703002 [hep-ph].

[46] M. Lev and B. Petersson, "Nuclear Effects at Large Transverse Momentum in a QCD Parton Model", *Z. Phys.* **C21** (1983) 155.

[47] X.-N. Wang, "Systematic study of high p_T hadron spectra in pp, p A and A A collisions from SPS to RHIC energies", *Phys. Rev.* **C61** (2000) 064910, arXiv:nucl-th/9812021 [nucl-th].

[48] B. Z. Kopeliovich, J. Nemchik, A. Schafer, and A. V. Tarasov, "Cronin effect in hadron production off nuclei", *Phys. Rev. Lett.* **88** (2002) 232303, arXiv:hep-ph/0201010 [hep-ph].

[49] **CMS** Collaboration, S. Chatrchyan *et al.*, "Observation of Long-Range Near-Side Angular Correlations in Proton-Lead Collisions at the LHC", *Phys. Lett.* **B718** (2013) 795–814, arXiv:1210.5482 [nucl-ex].

[50] **ALICE** Collaboration, B. Abelev *et al.*, "Long-range angular correlations on the near and away side in p–Pb collisions at $\sqrt{s_{NN}} = 5.02$ TeV", *Phys. Lett.* **B719** (2013) 29–41, arXiv:1212.2001 [nucl-ex].

[51] **ALICE** Collaboration, B. Abelev *et al.*, "Long-range angular correlations of π, K and p in p–Pb collisions at $\sqrt{s_{\rm NN}}$ = 5.02 TeV", *Phys. Lett.* **B726** (2013) 164–177, arXiv:1307.3237 [nucl-ex].

[52] **ALICE** Collaboration, J. Adam *et al.*, "Forward-central two-particle correlations in p–Pb collisions at $\sqrt{s_{\rm NN}}$ = 5.02 TeV", *Phys. Lett.* **B753** (2016) 126–139, arXiv:1506.08032 [nucl-ex].

[53] **ALICE** Collaboration, S. Acharya *et al.*, "Multiplicity dependence of light-flavor hadron production in pp collisions at $\sqrt{s}$ = 7 TeV", *Phys. Rev. C* **99** no. 2, (2019) 024906, arXiv:1807.11321 [nucl-ex].

[54] **ALICE** Collaboration, S. Acharya *et al.*, "Multiplicity dependence of π, K, and p production in pp collisions at $\sqrt{s} = 13$ TeV", *Eur. Phys. J. C* **80** no. 8, (2020) 693, arXiv:2003.02394 [nucl-ex].

[55] **ALICE** Collaboration, J. Adam *et al.*, "Multiplicity dependence of charged pion, kaon, and (anti)proton production at large transverse momentum in p-Pb collisions at $\sqrt{s_{\rm NN}}$ = 5.02 TeV", *Phys. Lett.* **B760** (2016) 720–735, arXiv:1601.03658 [nucl-ex].

[56] J. L. Nagle and W. A. Zajc, "Small System Collectivity in Relativistic Hadronic and Nuclear Collisions", *Ann. Rev. Nucl. Part. Sci.* **68** (2018) 211–235, arXiv:1801.03477 [nucl-ex].

[57] K. J. Eskola, H. Paukkunen, and C. A. Salgado, "EPS09: A New Generation of NLO and LO Nuclear Parton Distribution Functions", *JHEP* **04** (2009) 065, arXiv:0902.4154 [hep-ph].

[58] A. Beraudo, A. De Pace, M. Monteno, M. Nardi, and F. Prino, "Heavy-flavour production in high-energy d-Au and p-Pb collisions", *JHEP* **03** (2016) 123, arXiv:1512.05186 [hep-ph].

[59] **LHCb** Collaboration, R. Aaij *et al.*, "Prompt Λ_c^+ production in$p$Pb collisions at $\sqrt{s_{NN}} = 5.02$ TeV", *JHEP* **02** (2019) 102, arXiv:1809.01404 [hep-ex].

[60] M. He and R. Rapp, "Charm-baryon production in proton-proton collisions", *Physics Letters B* **795** (2019) 117–121, arXiv:1902.08889 [nucl-th].

[61] J. Song, H.-h. Li, and F.-l. Shao, "New feature of low p_T charm quark hadronization in pp collisions at $\sqrt{s} = 7$ TeV", *Eur. Phys. J.* **C78** no. 4, (2018) 344, arXiv:1801.09402 [hep-ph].

[62] H.-H. Li, F.-L. Shao, J. Song, and R.-Q. Wang, "Production of single-charm hadrons by quark combination mechanism in p-Pb collisions at $\sqrt{s_{NN}} = 5.02$ TeV", *Phys. Rev.* **C97** no. 6, (2018) 064915, arXiv:1712.08921 [hep-ph].

[63] **ALICE** Collaboration, S. Acharya *et al.*, "Measurement of D-meson production at mid-rapidity in pp collisions at $\sqrt{\mathbf{s}} = \mathbf{7}$ TeV", *Eur. Phys. J.* **C77** no. 8, (2017) 550, arXiv:1702.00766 [hep-ex].

[64] **ALICE** Collaboration, J. Adam *et al.*, "D-meson production in p–Pb collisions at $\sqrt{s_{\rm NN}} = 5.02$ TeV and in pp collisions at $\sqrt{s} = 7$ TeV", *Phys. Rev.* **C94** no. 5, (2016) 054908, arXiv:1605.07569 [nucl-ex].

[65] **ALICE** Collaboration, S. Acharya *et al.*, "Measurement of $\rm D^0$, $\rm D^+$, $\rm D^{*+}$ and $\rm D_s^+$ production in Pb-Pb collisions at $\sqrt{s_{\rm NN}} = 5.02$ TeV", *JHEP* **10** (2018) 174, arXiv:1804.09083 [nucl-ex].

[66] **ALICE** Collaboration, B. Abelev *et al.*, "Measurement of charm production at central rapidity in proton-proton collisions at $\sqrt{s} = 7$ TeV", *JHEP* **01** (2012) 128, arXiv:1111.1553 [hep-ex].

[67] **ALICE** Collaboration, B. Abelev *et al.*, "D_s^+ meson production at central rapidity in proton–proton collisions at $\sqrt{s} = 7$ TeV", *Phys. Lett.* **B718** (2012) 279–294, arXiv:1208.1948 [hep-ex].

[68] **ALICE** Collaboration, B. Abelev *et al.*, "Measurement of charm production at central rapidity in proton-proton collisions at $\sqrt{s} = 2.76$ TeV", *JHEP* **07** (2012) 191, arXiv:1205.4007 [hep-ex].

[69] **ALICE** Collaboration, S. Acharya *et al.*, "Λ_c^+ production and baryon-to-meson ratios in pp and p-Pb collisions at $\sqrt{s_{NN}}$ = 5.02 TeV at the LHC",. https://cds.cern.ch/record/2743731. CERN-EP-2020-217.

[70] **ALICE** Collaboration, K. Aamodt *et al.*, "The ALICE experiment at the CERN LHC", *JINST* **3** (2008) S08002.

[71] **ALICE** Collaboration, B. Abelev *et al.*, "Performance of the ALICE Experiment at the CERN LHC", *Int. J. Mod. Phys.* **A29** (2014) 1430044, `arXiv:1402.4476 [nucl-ex]`.

[72] **ALICE** Collaboration, K. Aamodt *et al.*, "Alignment of the ALICE Inner Tracking System with cosmic-ray tracks", *JINST* **5** (2010) P03003, `arXiv:1001.0502 [physics.ins-det]`.

[73] J. Alme *et al.*, "The ALICE TPC, a large 3-dimensional tracking device with fast readout for ultra-high multiplicity events", *Nucl. Instrum. Meth. A* **622** (2010) 316–367, `arXiv:1001.1950 [physics.ins-det]`.

[74] **ALICE** Collaboration, J. Adam *et al.*, "Determination of the event collision time with the ALICE detector at the LHC", *Eur. Phys. J. Plus* **132** no. 2, (2017) 99, `arXiv:1610.03055 [physics.ins-det]`.

[75] **ALICE** Collaboration, S. Acharya *et al.*, "ALICE 2017 luminosity determination for pp collisions at $\sqrt{s}$ = 5 TeV",. `https://cds.cern.ch/record/2648933`. ALICE-PUBLIC-2018-014.

[76] **ALICE** Collaboration, B. Abelev *et al.*, "Measurement of visible cross sections in proton-lead collisions at $\sqrt{s_{\rm NN}}$ = 5.02 TeV in van der Meer scans with the ALICE detector", *JINST* **9** no. 11, (2014) P11003, `arXiv:1405.1849 [nucl-ex]`.

[77] **Particle Data Group** Collaboration, P. A. Zyla *et al.*, "Review of Particle Physics", *Progress of Theoretical and Experimental Physics* **2020** . 083C01 (2020).

[78] **ALICE** Collaboration, J. Adam *et al.*, "Particle identification in ALICE: a Bayesian approach", *Eur. Phys. J. Plus* **131** no. 5, (2016) 168, `arXiv:1602.01392 [physics.data-an]`.

[79] A. Höcker, P. Speckmayer, J. Stelzer, J. Therhaag, E. von Toerne, and H. Voss, "TMVA: Toolkit for Multivariate Data Analysis", *PoS* **ACAT** (2007) 040, `arXiv:physics/0703039`.

[80] T. Sjöstrand, S. Mrenna, and P. Z. Skands, "PYTHIA 6.4 Physics and Manual", *JHEP* **05** (2006) 026, `arXiv:hep-ph/0603175 [hep-ph]`.

[81] P. Z. Skands, "The Perugia Tunes", in *Proceedings, 1st International Workshop on Multiple Partonic Interactions at the LHC (MPI08): Perugia, Italy, October 27-31, 2008*, pp. 284–297. 2009. `arXiv:0905.3418 [hep-ph]`.

[82] X.-N. Wang and M. Gyulassy, "HIJING: A Monte Carlo model for multiple jet production in pp, pA and AA collisions", *Phys. Rev.* **D44** (1991) 3501–3516.

[83] T. Sjöstrand, S. Mrenna, and P. Z. Skands, "A Brief Introduction to PYTHIA 8.1", *Comput. Phys. Commun.* **178** (2008) 852–867, `arXiv:0710.3820 [hep-ph]`.

[84] S. Frixione, P. Nason, and G. Ridolfi, "A Positive-weight next-to-leading-order Monte Carlo for heavy flavour hadroproduction", *JHEP* **09** (2007) 126, `arXiv:0707.3088 [hep-ph]`.

[85] S. Dulat, T.-J. Hou, J. Gao, M. Guzzi, J. Huston, P. Nadolsky, J. Pumplin, C. Schmidt, D. Stump, and C. P. Yuan, "New parton distribution functions from a global analysis of quantum chromodynamics", *Phys. Rev.* **D93** no. 3, (2016) 033006, `arXiv:1506.07443 [hep-ph]`.

[86] B. Kniehl, G. Kramer, I. Schienbein, and H. Spiesberger, "$\Lambda_c^{\pm}$ production in pp collisions with a new fragmentation function", *Phys. Rev. D* **101** (2020) 114021, `arXiv:2004.04213 [hep-ph]`.

[87] **OPAL** Collaboration, G. Alexander *et al.*, "A Study of charm hadron production in $Z^0 \to c\bar{c}$ and $Z^0 \to b\bar{b}$ decays at LEP", *Z. Phys.* **C72** (1996) 1–16.

[88] **Belle** Collaboration, M. Niiyama *et al.*, "Production cross sections of hyperons and charmed baryons from e^+e^- annihilation near $\sqrt{s} = 10.52$~GeV", *Phys. Rev. D* **97** no. 7, (2018) 072005, arXiv:1706.06791 [hep-ex].

[89] **ALICE** Collaboration, S. Acharya *et al.*, "Measurement of D^0 , D^+ , D^{*+} and D_s^+ production in pp collisions at $\sqrt{s} = 5.02$ TeV with ALICE", *Eur. Phys. J.* **C79** no. 5, (2019) 388, arXiv:1901.07979 [nucl-ex].

[90] **ALICE** Collaboration, S. Acharya *et al.*, "Measurement of prompt D^0, D^+, D^{*+}, and D_S^+ production in p–Pb collisions at $\sqrt{s_{NN}}$ = 5.02 TeV", *JHEP* **12** (2019) 092, arXiv:1906.03425 [nucl-ex].

[91] C. Bierlich, G. Gustafson, L. Lönnblad, and A. Tarasov, "Effects of Overlapping Strings in pp Collisions", *JHEP* **03** (2015) 148, arXiv:1412.6259 [hep-ph].

[92] D. Ebert, R. Faustov, and V. Galkin, "Spectroscopy and Regge trajectories of heavy baryons in the relativistic quark-diquark picture", *Phys. Rev. D* **84** (2011) 014025, arXiv:1105.0583 [hep-ph].

[93] S. Plumari, V. Minissale, S. K. Das, G. Coci, and V. Greco, "Charmed Hadrons from Coalescence plus Fragmentation in relativistic nucleus-nucleus collisions at RHIC and LHC", *Eur. Phys. J.* **C78** no. 4, (2018) 348, arXiv:1712.00730 [hep-ph].

[94] **ALICE** Collaboration, S. Acharya *et al.*, "Production of charged pions, kaons and (anti-)protons in Pb-Pb and inelastic pp collisions at $\sqrt{s_{NN}}$ = 5.02 TeV", *Phys. Rev. C* **101** no. 4, (2020) 044907, arXiv:1910.07678 [nucl-ex].

[95] **ALICE** Collaboration, B. B. Abelev *et al.*, "K_S^0 and Λ production in Pb-Pb collisions at $\sqrt{s_{NN}}$ = 2.76 TeV", *Phys. Rev. Lett.* **111** (2013) 222301, arXiv:1307.5530 [nucl-ex].

[96] **ALICE** Collaboration, B. Abelev *et al.*, "Multiplicity Dependence of Pion, Kaon, Proton and Lambda Production in p–Pb Collisions at $\sqrt{s_{NN}}$ = 5.02 TeV", *Phys. Lett.* **B728** (2014) 25–38, arXiv:1307.6796 [nucl-ex].

[97] **ALICE** Collaboration, B. Abelev *et al.*, "Upgrade of the ALICE Experiment: Letter Of Intent", *J. Phys.* **G41** (2014) 087001.

A The ALICE Collaboration

S. Acharya[142], D. Adamová[97], A. Adler[75], J. Adolfsson[82], G. Aglieri Rinella[35], M. Agnello[31], N. Agrawal[55], Z. Ahammed[142], S. Ahmad[16], S.U. Ahn[77], Z. Akbar[52], A. Akindinov[94], M. Al-Turany[109], D.S.D. Albuquerque[124], D. Aleksandrov[90], B. Alessandro[60], H.M. Alfanda[7], R. Alfaro Molina[72], B. Ali[16], Y. Ali[14], A. Alici[26], N. Alizadehvandchali[127], A. Alkin[35], J. Alme[21], T. Alt[69], L. Altenkamper[21], I. Altsybeev[115], M.N. Anaam[7], C. Andrei[49], D. Andreou[92], A. Andronic[145], M. Angeletti[35], V. Anguelov[106], T. Antičić[110], F. Antinori[58], P. Antonioli[55], N. Apadula[81], L. Aphecetche[117], H. Appelshäuser[69], S. Arcelli[26], R. Arnaldi[60], M. Arratia[81], I.C. Arsene[20], M. Arslandok[147,106], A. Augustinus[35], R. Averbeck[109], S. Aziz[79], M.D. Azmi[16], A. Badalà[57], Y.W. Baek[42], X. Bai[109], R. Bailhache[69], R. Bala[103], A. Balbino[31], A. Baldisseri[139], M. Ball[44], D. Banerjee[4], R. Barbera[27], L. Barioglio[25], M. Barlou[86], G.G. Barnaföldi[146], L.S. Barnby[96], V. Barret[136], C. Bartels[129], K. Barth[35], E. Bartsch[69], F. Baruffaldi[28], N. Bastid[136], S. Basu[82,144], G. Batigne[117], B. Batyunya[76], D. Bauri[50], J.L. Bazo Alba[114], I.G. Bearden[91], C. Beattie[147], I. Belikov[138], A.D.C. Bell Hechavarria[145], F. Bellini[35], R. Bellwied[127], S. Belokurova[115], V. Belyaev[95], G. Bencedi[70,146], S. Beole[25], A. Bercuci[49], Y. Berdnikov[100], A. Berdnikova[106], D. Berenyi[146], L. Bergmann[106], M.G. Besoiu[68], L. Betev[35], P.P. Bhaduri[142], A. Bhasin[103], I.R. Bhat[103], M.A. Bhat[4], B. Bhattacharjee[43], P. Bhattacharya[23], A. Bianchi[25], L. Bianchi[25], N. Bianchi[53], J. Bielčík[38], J. Bielčíková[97], A. Bilandzic[107], G. Biro[146], S. Biswas[4], J.T. Blair[121], D. Blau[90], M.B. Blidaru[109], C. Blume[69], G. Boca[29], F. Bock[98], A. Bogdanov[95], S. Boi[23], J. Bok[62], L. Boldizsár[146], A. Bolozdynya[95], M. Bombara[39], G. Bonomi[141], H. Borel[139], A. Borissov[83,95], H. Bossi[147], E. Botta[25], L. Bratrud[69], P. Braun-Munzinger[109], M. Bregant[123], M. Broz[38], G.E. Bruno[108,34], M.D. Buckland[129], D. Budnikov[111], H. Buesching[69], S. Bufalino[31], O. Bugnon[117], P. Buhler[116], P. Buncic[35], Z. Buthelezi[73,133], J.B. Butt[14], S.A. Bysiak[120], D. Caffarri[92], A. Caliva[109], E. Calvo Villar[114], J.M.M. Camacho[122], R.S. Camacho[46], P. Camerini[24], F.D.M. Canedo[123], A.A. Capon[116], F. Carnesecchi[26], R. Caron[139], J. Castillo Castellanos[139], E.A.R. Casula[56], F. Catalano[31], C. Ceballos Sanchez[76], P. Chakraborty[50], S. Chandra[142], W. Chang[7], S. Chapeland[35], M. Chartier[129], S. Chattopadhyay[142], S. Chattopadhyay[112], A. Chauvin[23], C. Cheshkov[137], B. Cheynis[137], V. Chibante Barroso[35], D.D. Chinellato[124], S. Cho[62], P. Chochula[35], P. Christakoglou[92], C.H. Christensen[91], P. Christiansen[82], T. Chujo[135], C. Cicalo[56], L. Cifarelli[26], F. Cindolo[55], M.R. Ciupek[109], G. Clai[II,55], J. Cleymans[126], F. Colamaria[54], J.S. Colburn[113], D. Colella[54], A. Collu[81], M. Colocci[35,26], M. Concas[III,60], G. Conesa Balbastre[80], Z. Conesa del Valle[79], G. Contin[24], J.G. Contreras[38], T.M. Cormier[98], P. Cortese[32], M.R. Cosentino[125], F. Costa[35], S. Costanza[29], P. Crochet[136], E. Cuautle[70], P. Cui[7], L. Cunqueiro[98], T. Dahms[107], A. Dainese[58], F.P.A. Damas[117,139], M.C. Danisch[106], A. Danu[68], D. Das[112], I. Das[112], P. Das[88], P. Das[4], S. Das[4], S. Dash[50], S. De[88], A. De Caro[30], G. de Cataldo[54], L. De Cilladi[25], J. de Cuveland[40], A. De Falco[23], D. De Gruttola[30], N. De Marco[60], C. De Martin[24], S. De Pasquale[30], S. Deb[51], H.F. Degenhardt[123], K.R. Deja[143], S. Delsanto[25], W. Deng[7], P. Dhankher[19,50], D. Di Bari[34], A. Di Mauro[35], R.A. Diaz[8], T. Dietel[126], P. Dillenseger[69], Y. Ding[7], R. Divià[35], D.U. Dixit[19], Ø. Djuvsland[21], U. Dmitrieva[64], J. Do[62], A. Dobrin[68], B. Dönigus[69], O. Dordic[20], A.K. Dubey[142], A. Dubla[109,92], S. Dudi[102], M. Dukhishyam[88], P. Dupieux[136], T.M. Eder[145], R.J. Ehlers[98], V.N. Eikeland[21], D. Elia[54], B. Erazmus[117], F. Erhardt[101], A. Erokhin[115], M.R. Ersdal[21], B. Espagnon[79], G. Eulisse[35], D. Evans[113], S. Evdokimov[93], L. Fabbietti[107], M. Faggin[28], J. Faivre[80], F. Fan[7], A. Fantoni[53], M. Fasel[98], P. Fecchio[31], A. Feliciello[60], G. Feofilov[115], A. Fernández Téllez[46], A. Ferrero[139], A. Ferretti[25], A. Festanti[35], V.J.G. Feuillard[106], J. Figiel[120], S. Filchagin[111], D. Finogeev[64], F.M. Fionda[21], G. Fiorenza[54], F. Flor[127], A.N. Flores[121], S. Foertsch[73], P. Foka[109], S. Fokin[90], E. Fragiacomo[61], U. Fuchs[35], C. Furget[80], A. Furs[64], M. Fusco Girard[30], J.J. Gaardhøje[91], M. Gagliardi[25], A.M. Gago[114], A. Gal[138], C.D. Galvan[122], P. Ganoti[86], C. Garabatos[109], J.R.A. Garcia[46], E. Garcia-Solis[10], K. Garg[117], C. Gargiulo[35], A. Garibli[89], K. Garner[145], P. Gasik[107], E.F. Gauger[121], M.B. Gay Ducati[71], M. Germain[117], J. Ghosh[112], P. Ghosh[142], S.K. Ghosh[4], M. Giacalone[26], P. Gianotti[53], P. Giubellino[109,60], P. Giubilato[28], A.M.C. Glaenzer[139], P. Glässel[106], V. Gonzalez[144], L.H. González-Trueba[72], S. Gorbunov[40], L. Görlich[120], S. Gotovac[36], V. Grabski[72], L.K. Graczykowski[143], K.L. Graham[113], L. Greiner[81], A. Grelli[63], C. Grigoras[35], V. Grigoriev[95], A. Grigoryan[I,1], S. Grigoryan[76], O.S. Groettvik[21], F. Grosa[60], J.F. Grosse-Oetringhaus[35], R. Grosso[109], R. Guernane[80], M. Guilbaud[117], M. Guittiere[117], K. Gulbrandsen[91], T. Gunji[134], A. Gupta[103], R. Gupta[103], I.B. Guzman[46], R. Haake[147], M.K. Habib[109], C. Hadjidakis[79], H. Hamagaki[84], G. Hamar[146], M. Hamid[7], R. Hannigan[121], M.R. Haque[143,88], A. Harlenderova[109], J.W. Harris[147], A. Harton[10], J.A. Hasenbichler[35], H. Hassan[98], D. Hatzifotiadou[55], P. Hauer[44], L.B. Havener[147], S. Hayashi[134], S.T. Heckel[107], E. Hellbär[69], H. Helstrup[37], T. Herman[38], E.G. Hernandez[46], G. Herrera Corral[9], F. Herrmann[145], K.F. Hetland[37], H. Hillemanns[35], C. Hills[129], B. Hippolyte[138], B. Hohlweger[107], J. Honermann[145], G.H. Hong[148], D. Horak[38], S. Hornung[109], R. Hosokawa[15], P. Hristov[35], C. Huang[79], C. Hughes[132], P. Huhn[69], T.J. Humanic[99], H. Hushnud[112], L.A. Husova[145], N. Hussain[43], D. Hutter[40], J.P. Iddon[35,129], R. Ilkaev[111], H. Ilyas[14], M. Inaba[135], G.M. Innocenti[35], M. Ippolitov[90], A. Isakov[38,97], M.S. Islam[112], M. Ivanov[109], V. Ivanov[100], V. Izucheev[93],

B. Jacak[81], N. Jacazio[35,55], P.M. Jacobs[81], S. Jadlovska[119], J. Jadlovsky[119], S. Jaelani[63], C. Jahnke[123], M.J. Jakubowska[143], M.A. Janik[143], T. Janson[75], M. Jercic[101], O. Jevons[113], M. Jin[127], F. Jonas[98,145], P.G. Jones[113], J. Jung[69], M. Jung[69], A. Jusko[113], P. Kalinak[65], A. Kalweit[35], V. Kaplin[95], S. Kar[7], A. Karasu Uysal[78], D. Karatovic[101], O. Karavichev[64], T. Karavicheva[64], P. Karczmarczyk[143], E. Karpechev[64], A. Kazantsev[90], U. Kebschull[75], R. Keidel[48], M. Keil[35], B. Ketzer[44], Z. Khabanova[92], A.M. Khan[7], S. Khan[16], A. Khanzadeev[100], Y. Kharlov[93], A. Khatun[16], A. Khuntia[120], B. Kileng[37], B. Kim[62], D. Kim[148], D.J. Kim[128], E.J. Kim[74], H. Kim[17], J. Kim[148], J.S. Kim[42], J. Kim[106], J. Kim[148], J. Kim[74], M. Kim[106], S. Kim[18], T. Kim[148], T. Kim[148], S. Kirsch[69], I. Kisel[40], S. Kiselev[94], A. Kisiel[143], J.L. Klay[6], J. Klein[35,60], S. Klein[81], C. Klein-Bösing[145], M. Kleiner[69], T. Klemenz[107], A. Kluge[35], A.G. Knospe[127], C. Kobdaj[118], M.K. Köhler[106], T. Kollegger[109], A. Kondratyev[76], N. Kondratyeva[95], E. Kondratyuk[93], J. Konig[69], S.A. Konigstorfer[107], P.J. Konopka[2,35], G. Kornakov[143], S.D. Koryciak[2], L. Koska[119], O. Kovalenko[87], V. Kovalenko[115], M. Kowalski[120], I. Králik[65], A. Kravčáková[39], L. Kreis[109], M. Krivda[113,65], F. Krizek[97], K. Krizkova Gajdosova[38], M. Kroesen[106], M. Krüger[69], E. Kryshen[100], M. Krzewicki[40], V. Kučera[35], C. Kuhn[138], P.G. Kuijer[92], T. Kumaoka[135], L. Kumar[102], S. Kundu[88], P. Kurashvili[87], A. Kurepin[64], A.B. Kurepin[64], A. Kuryakin[111], S. Kushpil[97], J. Kvapil[113], M.J. Kweon[62], J.Y. Kwon[62], Y. Kwon[148], S.L. La Pointe[40], P. La Rocca[27], Y.S. Lai[81], A. Lakrathok[118], M. Lamanna[35], R. Langoy[131], K. Lapidus[35], P. Larionov[53], E. Laudi[35], L. Lautner[35], R. Lavicka[38], T. Lazareva[115], R. Lea[24], J. Lee[135], S. Lee[148], J. Lehrbach[40], R.C. Lemmon[96], I. León Monzón[122], E.D. Lesser[19], M. Lettrich[35], P. Lévai[146], X. Li[11], X.L. Li[7], J. Lien[131], R. Lietava[113], B. Lim[17], S.H. Lim[17], V. Lindenstruth[40], A. Lindner[49], C. Lippmann[109], A. Liu[19], J. Liu[129], I.M. Lofnes[21], V. Loginov[95], C. Loizides[98], P. Loncar[36], J.A. Lopez[106], X. Lopez[136], E. López Torres[8], J.R. Luhder[145], M. Lunardon[28], G. Luparello[61], Y.G. Ma[41], A. Maevskaya[64], M. Mager[35], S.M. Mahmood[20], T. Mahmoud[44], A. Maire[138], R.D. Majka[I,147], M. Malaev[100], Q.W. Malik[20], L. Malinina[IV,76], D. Mal'Kevich[94], N. Mallick[51], P. Malzacher[109], G. Mandaglio[33,57], V. Manko[90], F. Manso[136], V. Manzari[54], Y. Mao[7], M. Marchisone[137], J. Mareš[67], G.V. Margagliotti[24], A. Margotti[55], A. Marín[109], C. Markert[121], M. Marquard[69], N.A. Martin[106], P. Martinengo[35], J.L. Martinez[127], M.I. Martínez[46], G. Martínez García[117], S. Masciocchi[109], M. Masera[25], A. Masoni[56], L. Massacrier[79], A. Mastroserio[140,54], A.M. Mathis[107], O. Matonoha[82], P.F.T. Matuoka[123], A. Matyja[120], C. Mayer[120], F. Mazzaschi[25], M. Mazzilli[54], M.A. Mazzoni[59], A.F. Mechler[69], F. Meddi[22], Y. Melikyan[64], A. Menchaca-Rocha[72], C. Mengke[7], E. Meninno[116,30], A.S. Menon[127], M. Meres[13], S. Mhlanga[126], Y. Miake[135], L. Micheletti[25], L.C. Migliorin[137], D.L. Mihaylov[107], K. Mikhaylov[76,94], A.N. Mishra[146,70], D. Miśkowiec[109], A. Modak[4], N. Mohammadi[35], A.P. Mohanty[63], B. Mohanty[88], M. Mohisin Khan[16], Z. Moravcova[91], C. Mordasini[107], D.A. Moreira De Godoy[145], L.A.P. Moreno[46], I. Morozov[64], A. Morsch[35], T. Mrnjavac[35], V. Muccifora[53], E. Mudnic[36], D. Mühlheim[145], S. Muhuri[142], J.D. Mulligan[81], A. Mulliri[23,56], M.G. Munhoz[123], R.H. Munzer[69], H. Murakami[134], S. Murray[126], L. Musa[35], J. Musinsky[65], C.J. Myers[127], J.W. Myrcha[143], B. Naik[50], R. Nair[87], B.K. Nandi[50], R. Nania[55], E. Nappi[54], M.U. Naru[14], A.F. Nassirpour[82], C. Nattrass[132], R. Nayak[50], S. Nazarenko[111], A. Neagu[20], L. Nellen[70], S.V. Nesbo[37], G. Neskovic[40], D. Nesterov[115], B.S. Nielsen[91], S. Nikolaev[90], S. Nikulin[90], V. Nikulin[100], F. Noferini[55], S. Noh[12], P. Nomokonov[76], J. Norman[129], N. Novitzky[135], P. Nowakowski[143], A. Nyanin[90], J. Nystrand[21], M. Ogino[84], A. Ohlson[82], J. Oleniacz[143], A.C. Oliveira Da Silva[132], M.H. Oliver[147], B.S. Onnerstad[128], C. Oppedisano[60], A. Ortiz Velasquez[70], T. Osako[47], A. Oskarsson[82], J. Otwinowski[120], K. Oyama[84], Y. Pachmayer[106], S. Padhan[50], D. Pagano[141], G. Paić[70], J. Pan[144], S. Panebianco[139], P. Pareek[142], J. Park[62], J.E. Parkkila[128], S. Parmar[102], S.P. Pathak[127], B. Paul[23], J. Pazzini[141], H. Pei[7], T. Peitzmann[63], X. Peng[7], L.G. Pereira[71], H. Pereira Da Costa[139], D. Peresunko[90], G.M. Perez[8], S. Perrin[139], Y. Pestov[5], V. Petráček[38], M. Petrovici[49], R.P. Pezzi[71], S. Piano[61], M. Pikna[13], P. Pillot[117], O. Pinazza[55,35], L. Pinsky[127], C. Pinto[27], S. Pisano[53], M. Płoskoń[81], M. Planinic[101], F. Pliquett[69], M.G. Poghosyan[98], B. Polichtchouk[93], N. Poljak[101], A. Pop[49], S. Porteboeuf-Houssais[136], J. Porter[81], V. Pozdniakov[76], S.K. Prasad[4], R. Preghenella[55], F. Prino[60], C.A. Pruneau[144], I. Pshenichnov[64], M. Puccio[35], S. Qiu[92], L. Quaglia[25], R.E. Quishpe[127], S. Ragoni[113], J. Rak[128], A. Rakotozafindrabe[139], L. Ramello[32], F. Rami[138], S.A.R. Ramirez[46], A.G.T. Ramos[34], R. Raniwala[104], S. Raniwala[104], S.S. Räsänen[45], R. Rath[51], I. Ravasenga[92], K.F. Read[98,132], A.R. Redelbach[40], K. Redlich[V,87], A. Rehman[21], P. Reichelt[69], F. Reidt[35], R. Renfordt[69], Z. Rescakova[39], K. Reygers[106], A. Riabov[100], V. Riabov[100], T. Richert[82,91], M. Richter[20], P. Riedler[35], W. Riegler[35], F. Riggi[27], C. Ristea[68], S.P. Rode[51], M. Rodríguez Cahuantzi[46], K. Røed[20], R. Rogalev[93], E. Rogochaya[76], T.S. Rogoschinski[69], D. Rohr[35], D. Röhrich[21], P.F. Rojas[46], P.S. Rokita[143], F. Ronchetti[53], A. Rosano[33,57], E.D. Rosas[70], A. Rossi[58], A. Rotondi[29], A. Roy[51], P. Roy[112], O.V. Rueda[82], R. Rui[24], B. Rumyantsev[76], A. Rustamov[89], E. Ryabinkin[90], Y. Ryabov[100], A. Rybicki[120], H. Rytkonen[128], O.A.M. Saarimaki[45], R. Sadek[117], S. Sadovsky[93], J. Saetre[21], K. Šafařík[38], S.K. Saha[142], S. Saha[88], B. Sahoo[50], P. Sahoo[50], R. Sahoo[51], S. Sahoo[66], D. Sahu[51], P.K. Sahu[66], J. Saini[142], S. Sakai[135], S. Sambyal[103], V. Samsonov[100,95], D. Sarkar[144], N. Sarkar[142], P. Sarma[43], V.M. Sarti[107], M.H.P. Sas[147,63],

J. Schambach[98,121], H.S. Scheid[69], C. Schiaua[49], R. Schicker[106], A. Schmah[106], C. Schmidt[109], H.R. Schmidt[105], M.O. Schmidt[106], M. Schmidt[105], N.V. Schmidt[98,69], A.R. Schmier[132], R. Schotter[138], J. Schukraft[35], Y. Schutz[138], K. Schwarz[109], K. Schweda[109], G. Scioli[26], E. Scomparin[60], J.E. Seger[15], Y. Sekiguchi[134], D. Sekihata[134], I. Selyuzhenkov[109,95], S. Senyukov[138], J.J. Seo[62], D. Serebryakov[64], L. Šerkšnytė[107], A. Sevcenco[68], A. Shabanov[64], A. Shabetai[117], R. Shahoyan[35], W. Shaikh[112], A. Shangaraev[93], A. Sharma[102], H. Sharma[120], M. Sharma[103], N. Sharma[102], S. Sharma[103], O. Sheibani[127], A.I. Sheikh[142], K. Shigaki[47], M. Shimomura[85], S. Shirinkin[94], Q. Shou[41], Y. Sibiriak[90], S. Siddhanta[56], T. Siemiarczuk[87], D. Silvermyr[82], G. Simatovic[92], G. Simonetti[35], B. Singh[107], R. Singh[88], R. Singh[103], R. Singh[51], V.K. Singh[142], V. Singhal[142], T. Sinha[112], B. Sitar[13], M. Sitta[32], T.B. Skaali[20], M. Slupecki[45], N. Smirnov[147], R.J.M. Snellings[63], C. Soncco[114], J. Song[127], A. Songmoolnak[118], F. Soramel[28], S. Sorensen[132], I. Sputowska[120], J. Stachel[106], I. Stan[68], P.J. Steffanic[132], S.F. Stiefelmaier[106], D. Stocco[117], M.M. Storetvedt[37], L.D. Stritto[30], C.P. Stylianidis[92], A.A.P. Suaide[123], T. Sugitate[47], C. Suire[79], M. Suljic[35], R. Sultanov[94], M. Šumbera[97], V. Sumberia[103], S. Sumowidagdo[52], S. Swain[66], A. Szabo[13], I. Szarka[13], U. Tabassam[14], S.F. Taghavi[107], G. Taillepied[136], J. Takahashi[124], G.J. Tambave[21], S. Tang[136,7], Z. Tang[130], M. Tarhini[117], M.G. Tarzila[49], A. Tauro[35], G. Tejeda Muñoz[46], A. Telesca[35], L. Terlizzi[25], C. Terrevoli[127], G. Tersimonov[3], S. Thakur[142], D. Thomas[121], F. Thoresen[91], R. Tieulent[137], A. Tikhonov[64], A.R. Timmins[127], M. Tkacik[119], A. Toia[69], N. Topilskaya[64], M. Toppi[53], F. Torales-Acosta[19], S.R. Torres[38,9], A. Trifiró[33,57], S. Tripathy[70], T. Tripathy[50], S. Trogolo[28], G. Trombetta[34], L. Tropp[39], V. Trubnikov[3], W.H. Trzaska[128], T.P. Trzcinski[143], B.A. Trzeciak[38], A. Tumkin[111], R. Turrisi[58], T.S. Tveter[20], K. Ullaland[21], E.N. Umaka[127], A. Uras[137], G.L. Usai[23], M. Vala[39], N. Valle[29], S. Vallero[60], N. van der Kolk[63], L.V.R. van Doremalen[63], M. van Leeuwen[92], P. Vande Vyvre[35], D. Varga[146], Z. Varga[146], M. Varga-Kofarago[146], A. Vargas[46], M. Vasileiou[86], A. Vasiliev[90], O. Vázquez Doce[107], V. Vechernin[115], E. Vercellin[25], S. Vergara Limón[46], L. Vermunt[63], R. Vértesi[146], M. Verweij[63], L. Vickovic[36], Z. Vilakazi[133], O. Villalobos Baillie[113], G. Vino[54], A. Vinogradov[90], T. Virgili[30], V. Vislavicius[91], A. Vodopyanov[76], B. Volkel[35], M.A. Völkl[105], K. Voloshin[94], S.A. Voloshin[144], G. Volpe[34], B. von Haller[35], I. Vorobyev[107], D. Voscek[119], J. Vrláková[39], B. Wagner[21], M. Weber[116], A. Wegrzynek[35], S.C. Wenzel[35], J.P. Wessels[145], J. Wiechula[69], J. Wikne[20], G. Wilk[87], J. Wilkinson[109], G.A. Willems[145], E. Willsher[113], B. Windelband[106], M. Winn[139], W.E. Witt[132], J.R. Wright[121], Y. Wu[130], R. Xu[7], S. Yalcin[78], Y. Yamaguchi[47], K. Yamakawa[47], S. Yang[21], S. Yano[47,139], Z. Yin[7], H. Yokoyama[63], I.-K. Yoo[17], J.H. Yoon[62], S. Yuan[21], A. Yuncu[106], V. Yurchenko[3], V. Zaccolo[24], A. Zaman[14], C. Zampolli[35], H.J.C. Zanoli[63], N. Zardoshti[35], A. Zarochentsev[115], P. Závada[67], N. Zaviyalov[111], H. Zbroszczyk[143], M. Zhalov[100], S. Zhang[41], X. Zhang[7], Y. Zhang[130], V. Zherebchevskii[115], Y. Zhi[11], D. Zhou[7], Y. Zhou[91], J. Zhu[7,109], Y. Zhu[7], A. Zichichi[26], G. Zinovjev[3], N. Zurlo[141]

Affiliation notes

[I] Deceased
[II] Also at: Italian National Agency for New Technologies, Energy and Sustainable Economic Development (ENEA), Bologna, Italy
[III] Also at: Dipartimento DET del Politecnico di Torino, Turin, Italy
[IV] Also at: M.V. Lomonosov Moscow State University, D.V. Skobeltsyn Institute of Nuclear, Physics, Moscow, Russia
[V] Also at: Institute of Theoretical Physics, University of Wroclaw, Poland

Collaboration Institutes

[1] A.I. Alikhanyan National Science Laboratory (Yerevan Physics Institute) Foundation, Yerevan, Armenia
[2] AGH University of Science and Technology, Cracow, Poland
[3] Bogolyubov Institute for Theoretical Physics, National Academy of Sciences of Ukraine, Kiev, Ukraine
[4] Bose Institute, Department of Physics and Centre for Astroparticle Physics and Space Science (CAPSS), Kolkata, India
[5] Budker Institute for Nuclear Physics, Novosibirsk, Russia
[6] California Polytechnic State University, San Luis Obispo, California, United States
[7] Central China Normal University, Wuhan, China
[8] Centro de Aplicaciones Tecnológicas y Desarrollo Nuclear (CEADEN), Havana, Cuba
[9] Centro de Investigación y de Estudios Avanzados (CINVESTAV), Mexico City and Mérida, Mexico
[10] Chicago State University, Chicago, Illinois, United States

[11] China Institute of Atomic Energy, Beijing, China
[12] Chungbuk National University, Cheongju, Republic of Korea
[13] Comenius University Bratislava, Faculty of Mathematics, Physics and Informatics, Bratislava, Slovakia
[14] COMSATS University Islamabad, Islamabad, Pakistan
[15] Creighton University, Omaha, Nebraska, United States
[16] Department of Physics, Aligarh Muslim University, Aligarh, India
[17] Department of Physics, Pusan National University, Pusan, Republic of Korea
[18] Department of Physics, Sejong University, Seoul, Republic of Korea
[19] Department of Physics, University of California, Berkeley, California, United States
[20] Department of Physics, University of Oslo, Oslo, Norway
[21] Department of Physics and Technology, University of Bergen, Bergen, Norway
[22] Dipartimento di Fisica dell'Università 'La Sapienza' and Sezione INFN, Rome, Italy
[23] Dipartimento di Fisica dell'Università and Sezione INFN, Cagliari, Italy
[24] Dipartimento di Fisica dell'Università and Sezione INFN, Trieste, Italy
[25] Dipartimento di Fisica dell'Università and Sezione INFN, Turin, Italy
[26] Dipartimento di Fisica e Astronomia dell'Università and Sezione INFN, Bologna, Italy
[27] Dipartimento di Fisica e Astronomia dell'Università and Sezione INFN, Catania, Italy
[28] Dipartimento di Fisica e Astronomia dell'Università and Sezione INFN, Padova, Italy
[29] Dipartimento di Fisica e Nucleare e Teorica, Università di Pavia and Sezione INFN, Pavia, Italy
[30] Dipartimento di Fisica 'E.R. Caianiello' dell'Università and Gruppo Collegato INFN, Salerno, Italy
[31] Dipartimento DISAT del Politecnico and Sezione INFN, Turin, Italy
[32] Dipartimento di Scienze e Innovazione Tecnologica dell'Università del Piemonte Orientale and INFN Sezione di Torino, Alessandria, Italy
[33] Dipartimento di Scienze MIFT, Università di Messina, Messina, Italy
[34] Dipartimento Interateneo di Fisica 'M. Merlin' and Sezione INFN, Bari, Italy
[35] European Organization for Nuclear Research (CERN), Geneva, Switzerland
[36] Faculty of Electrical Engineering, Mechanical Engineering and Naval Architecture, University of Split, Split, Croatia
[37] Faculty of Engineering and Science, Western Norway University of Applied Sciences, Bergen, Norway
[38] Faculty of Nuclear Sciences and Physical Engineering, Czech Technical University in Prague, Prague, Czech Republic
[39] Faculty of Science, P.J. Šafárik University, Košice, Slovakia
[40] Frankfurt Institute for Advanced Studies, Johann Wolfgang Goethe-Universität Frankfurt, Frankfurt, Germany
[41] Fudan University, Shanghai, China
[42] Gangneung-Wonju National University, Gangneung, Republic of Korea
[43] Gauhati University, Department of Physics, Guwahati, India
[44] Helmholtz-Institut für Strahlen- und Kernphysik, Rheinische Friedrich-Wilhelms-Universität Bonn, Bonn, Germany
[45] Helsinki Institute of Physics (HIP), Helsinki, Finland
[46] High Energy Physics Group, Universidad Autónoma de Puebla, Puebla, Mexico
[47] Hiroshima University, Hiroshima, Japan
[48] Hochschule Worms, Zentrum für Technologietransfer und Telekommunikation (ZTT), Worms, Germany
[49] Horia Hulubei National Institute of Physics and Nuclear Engineering, Bucharest, Romania
[50] Indian Institute of Technology Bombay (IIT), Mumbai, India
[51] Indian Institute of Technology Indore, Indore, India
[52] Indonesian Institute of Sciences, Jakarta, Indonesia
[53] INFN, Laboratori Nazionali di Frascati, Frascati, Italy
[54] INFN, Sezione di Bari, Bari, Italy
[55] INFN, Sezione di Bologna, Bologna, Italy
[56] INFN, Sezione di Cagliari, Cagliari, Italy
[57] INFN, Sezione di Catania, Catania, Italy
[58] INFN, Sezione di Padova, Padova, Italy
[59] INFN, Sezione di Roma, Rome, Italy
[60] INFN, Sezione di Torino, Turin, Italy
[61] INFN, Sezione di Trieste, Trieste, Italy
[62] Inha University, Incheon, Republic of Korea

[63] Institute for Gravitational and Subatomic Physics (GRASP), Utrecht University/Nikhef, Utrecht, Netherlands
[64] Institute for Nuclear Research, Academy of Sciences, Moscow, Russia
[65] Institute of Experimental Physics, Slovak Academy of Sciences, Košice, Slovakia
[66] Institute of Physics, Homi Bhabha National Institute, Bhubaneswar, India
[67] Institute of Physics of the Czech Academy of Sciences, Prague, Czech Republic
[68] Institute of Space Science (ISS), Bucharest, Romania
[69] Institut für Kernphysik, Johann Wolfgang Goethe-Universität Frankfurt, Frankfurt, Germany
[70] Instituto de Ciencias Nucleares, Universidad Nacional Autónoma de México, Mexico City, Mexico
[71] Instituto de Física, Universidade Federal do Rio Grande do Sul (UFRGS), Porto Alegre, Brazil
[72] Instituto de Física, Universidad Nacional Autónoma de México, Mexico City, Mexico
[73] iThemba LABS, National Research Foundation, Somerset West, South Africa
[74] Jeonbuk National University, Jeonju, Republic of Korea
[75] Johann-Wolfgang-Goethe Universität Frankfurt Institut für Informatik, Fachbereich Informatik und Mathematik, Frankfurt, Germany
[76] Joint Institute for Nuclear Research (JINR), Dubna, Russia
[77] Korea Institute of Science and Technology Information, Daejeon, Republic of Korea
[78] KTO Karatay University, Konya, Turkey
[79] Laboratoire de Physique des 2 Infinis, Irène Joliot-Curie, Orsay, France
[80] Laboratoire de Physique Subatomique et de Cosmologie, Université Grenoble-Alpes, CNRS-IN2P3, Grenoble, France
[81] Lawrence Berkeley National Laboratory, Berkeley, California, United States
[82] Lund University Department of Physics, Division of Particle Physics, Lund, Sweden
[83] Moscow Institute for Physics and Technology, Moscow, Russia
[84] Nagasaki Institute of Applied Science, Nagasaki, Japan
[85] Nara Women's University (NWU), Nara, Japan
[86] National and Kapodistrian University of Athens, School of Science, Department of Physics , Athens, Greece
[87] National Centre for Nuclear Research, Warsaw, Poland
[88] National Institute of Science Education and Research, Homi Bhabha National Institute, Jatni, India
[89] National Nuclear Research Center, Baku, Azerbaijan
[90] National Research Centre Kurchatov Institute, Moscow, Russia
[91] Niels Bohr Institute, University of Copenhagen, Copenhagen, Denmark
[92] Nikhef, National institute for subatomic physics, Amsterdam, Netherlands
[93] NRC Kurchatov Institute IHEP, Protvino, Russia
[94] NRC «Kurchatov»Institute - ITEP, Moscow, Russia
[95] NRNU Moscow Engineering Physics Institute, Moscow, Russia
[96] Nuclear Physics Group, STFC Daresbury Laboratory, Daresbury, United Kingdom
[97] Nuclear Physics Institute of the Czech Academy of Sciences, Řež u Prahy, Czech Republic
[98] Oak Ridge National Laboratory, Oak Ridge, Tennessee, United States
[99] Ohio State University, Columbus, Ohio, United States
[100] Petersburg Nuclear Physics Institute, Gatchina, Russia
[101] Physics department, Faculty of science, University of Zagreb, Zagreb, Croatia
[102] Physics Department, Panjab University, Chandigarh, India
[103] Physics Department, University of Jammu, Jammu, India
[104] Physics Department, University of Rajasthan, Jaipur, India
[105] Physikalisches Institut, Eberhard-Karls-Universität Tübingen, Tübingen, Germany
[106] Physikalisches Institut, Ruprecht-Karls-Universität Heidelberg, Heidelberg, Germany
[107] Physik Department, Technische Universität München, Munich, Germany
[108] Politecnico di Bari and Sezione INFN, Bari, Italy
[109] Research Division and ExtreMe Matter Institute EMMI, GSI Helmholtzzentrum für Schwerionenforschung GmbH, Darmstadt, Germany
[110] Rudjer Bošković Institute, Zagreb, Croatia
[111] Russian Federal Nuclear Center (VNIIEF), Sarov, Russia
[112] Saha Institute of Nuclear Physics, Homi Bhabha National Institute, Kolkata, India
[113] School of Physics and Astronomy, University of Birmingham, Birmingham, United Kingdom
[114] Sección Física, Departamento de Ciencias, Pontificia Universidad Católica del Perú, Lima, Peru
[115] St. Petersburg State University, St. Petersburg, Russia

[116] Stefan Meyer Institut für Subatomare Physik (SMI), Vienna, Austria
[117] SUBATECH, IMT Atlantique, Université de Nantes, CNRS-IN2P3, Nantes, France
[118] Suranaree University of Technology, Nakhon Ratchasima, Thailand
[119] Technical University of Košice, Košice, Slovakia
[120] The Henryk Niewodniczanski Institute of Nuclear Physics, Polish Academy of Sciences, Cracow, Poland
[121] The University of Texas at Austin, Austin, Texas, United States
[122] Universidad Autónoma de Sinaloa, Culiacán, Mexico
[123] Universidade de São Paulo (USP), São Paulo, Brazil
[124] Universidade Estadual de Campinas (UNICAMP), Campinas, Brazil
[125] Universidade Federal do ABC, Santo Andre, Brazil
[126] University of Cape Town, Cape Town, South Africa
[127] University of Houston, Houston, Texas, United States
[128] University of Jyväskylä, Jyväskylä, Finland
[129] University of Liverpool, Liverpool, United Kingdom
[130] University of Science and Technology of China, Hefei, China
[131] University of South-Eastern Norway, Tonsberg, Norway
[132] University of Tennessee, Knoxville, Tennessee, United States
[133] University of the Witwatersrand, Johannesburg, South Africa
[134] University of Tokyo, Tokyo, Japan
[135] University of Tsukuba, Tsukuba, Japan
[136] Université Clermont Auvergne, CNRS/IN2P3, LPC, Clermont-Ferrand, France
[137] Université de Lyon, CNRS/IN2P3, Institut de Physique des 2 Infinis de Lyon , Lyon, France
[138] Université de Strasbourg, CNRS, IPHC UMR 7178, F-67000 Strasbourg, France, Strasbourg, France
[139] Université Paris-Saclay Centre d'Etudes de Saclay (CEA), IRFU, Départment de Physique Nucléaire (DPhN), Saclay, France
[140] Università degli Studi di Foggia, Foggia, Italy
[141] Università di Brescia and Sezione INFN, Brescia, Italy
[142] Variable Energy Cyclotron Centre, Homi Bhabha National Institute, Kolkata, India
[143] Warsaw University of Technology, Warsaw, Poland
[144] Wayne State University, Detroit, Michigan, United States
[145] Westfälische Wilhelms-Universität Münster, Institut für Kernphysik, Münster, Germany
[146] Wigner Research Centre for Physics, Budapest, Hungary
[147] Yale University, New Haven, Connecticut, United States
[148] Yonsei University, Seoul, Republic of Korea